Sulfate-dependent anaerobic oxidation of methane at a highly dynamic bubbling site in the Eastern Sea of Marmara (Çinarcik Basin)

Barbara M. A. Teichert, Nicolas Chevalier, N. Gussone, Germain Bayon, Emmanuel Ponzevera, Livio Ruffine, Harald Strauss

Deep Sea Research Part II: Topical Studies in Oceanography
July 2018, Volume 153, Pages 79-91
http://dx.doi.org/10.1016/j.dsr2.2017.11.014
http://archimer.ifremer.fr/doc/00413/52480/

Sulfate-dependent anaerobic oxidation of methane at a highly dynamic bubbling site in the Eastern Sea of Marmara (Çinarcik Basin)

Teichert B.M.A. [1], Chevalier N. [1, 2], Gussone N. [3], Bayon Germain [4], Ponzevera Emmanuel [4], Ruffine Livio [4], Strauss H. [1]

[1] Institut für Geologie und Paläontologie, Westfälische Wilhelms-Universität Münster, Corrensstr. 24, 48149 Münster, Germany
[2] Sorbonne Universités, UPMC, University Paris 06, CNRS-IRD-MNHN, LOCEAN/IPSL Laboratory, 4 Place Jussieu, 75005 Paris, France
[3] Institut für Mineralogie, Westfälische Wilhelms-Universität Münster, Corrensstr. 24, 48149 Münster, Germany
[4] IFREMER, Département REM, Unité des Géosciences Marines, 29280 Plouzané, France

Abstract :

During the MARSITECruise expedition in November 2014 on board the RV *Pourquoi Pas*?, multidisciplinary sampling was carried out with the ROV Victor 6000 in order to investigate biogeochemical processes taking place at cold seep environments in the Sea of Marmara. Pore water, bottom water, sediment and authigenic carbonate samples were collected from two short push cores (MRS-DV5-PC04 − 8 cm, MRS-DV5-PC01 − 12.5 cm) at an active methane bubbling site in the southeastern part of the Çinarcik Basin. Sulfate sulfur and oxygen isotope data as well as sulfide isotope data indicate that sulfate-dependent anaerobic oxidation of methane is the dominant process in the sediments. This is confirmed by archaeal lipids diagnostic for anaerobic methane oxidizers detected with strong 13C-depletions. The available data even allows to distinguish the dominant AOM assemblages. Specific lipid patterns are consistent with a dominance of ANME-2 archaea within the microbial community. Abundant authigenic carbonates (mostly aragonite), found at all depths, show a narrow range in δ13C values between −27.69‰ and −33.40‰. The carbon isotopic composition of the dissolved inorganic carbon as well as strontium and calcium isotopes confirm that the current reaction zone (sulfate-methane transition zone) starts at the bottom of the core. All shallower carbonates are witnesses of paleo seepage activity. U-Th dating of four pure aragonite samples show the short time span that is preserved in core MRS-DV5-PC01 (235 ± 60 yr B.P.). Two major earthquakes of 1766 AD and 1754 AD in the Çinarcik Basin might potentially have triggered the increased seepage of methane at this location.

Keywords : Sea of Marmara, Çinarcik Basin, methane, sulfate reduction, anaerobic oxidation of methane, authigenic carbonate, lipid biomarker

1. Introduction

The Sea of Marmara (SoM) is strongly influenced by the northern branch of the North Anatolian Fault (NAF; Fig. 1). This major dextral fault system takes up about 20-25 mm/yr of strike-slip motion which is most of the motion between the Anatolian plate and Eurasian plate (Seeber et al., 2006). The SoM is characterized by three deep fault-bounded extensional basins with water depths of ~1.2 km (Tekirdağ, Central, and Çinarcik basins) separated by compressional ridges (Western High, Central High). Çinarcik Basin (Fig. 1) is a triangular half graben bordered to the north by the northern strand of the North Anatolian transform fault, which is a key element for Sea of Marmara tectonics and for seismic hazards in Istanbul and along this segment of the Turkish coastline (Seeber et al., 2006). Associated with these faults is an intensive seismicity and fluid emission activity at the seafloor. It has been suggested that at least some of these faults might channel fluids from deep levels and possibly from the seismogenic zone (Dupré et al., 2015; Zitter et al., 2008). In recent years, gas emissions from the seafloor into the water column of the Sea of Marmara have been investigated with the help of acoustic techniques (Bayrakci et al., 2014; Dupré et al., 2015; Géli et al., 2008). These studies have documented a strong correlation between gas emissions and present-day microseismic activity and between gas emissions and active faults although they are also associated to inactive faults (Dupré et al., 2015). The released gases are primarily of thermogenic origin in the western part of the sea, while mainly biogenic gases have been sampled in Çinarcik Basin and the Gulf of Izmit (Bourry et al., 2009; Ruffine et al., this issue). Related to the faults are cold seeps on the seafloor that are characterized by emanating gases and fluids. Associated with these environments are distinct geochemical gradients, microbial communities, macrofauna and authigenic carbonates. The latter ones have been sampled in the SoM on the seafloor but also from within sediment cores (Çağatay et al., this issue; Chevalier et al., 2011; 2010; Crémière et al., 2013; 2012). Molecular investigations of a seafloor carbonate from Çinarcik Basin confirmed that anaerobic oxidation of methane (AOM) associated with sulfate reduction appears to be a major biogeochemical process and that the microbial assemblage was dominated by ANME-2 archaea (Chevalier et al., 2013).

In this study, we sampled two push cores from the southeastern Çinarcik Basin at high resolution to investigate the biogeochemical processes in the shallow subsurface related to methane bubbling at the seafloor. We intend to identify the responsible microorganisms metabolizing the provided hydrocarbons and the evidence for this process in the pore waters. Authigenic carbonates precipitate within the sediments due to microbial activity and are therefore witnesses for microbial turnover processes. These will be investigated as archives not only for sub-recent but also past processes.

2. Study site

The study site (N 40°42.93520, E 29°06.83289) is located in the southeastern part of Çinarcik Basin (Fig. 1), in the Sea of Marmara. It is associated to en echelon normal faults that trend ~N130°-N140° and are distributed in a 2-4 km wide swath oriented N100° (Dupré et al., 2015). The water depth is 1239 m and the bottom water temperature was 14.5 °C at the time of sampling. The push cores were taken at a site of active gas bubbling through numerous holes of about 1-2 cm in diameter in the seafloor (Fig. 2). The color of the sediments was black indicating a sulfidic, anoxic environment and yellowish polychaetes (Fig. 3) were seen on the seafloor and later in the surface sediments (~1 cm long). Gas bubbling has been observed in this region also in previous studies (Dupré et al., 2015; Géli et al., 2008).

3. Materials

3.1 Sampling

The samples for this study were collected from two sediment push cores taken by the Remotely Operated Vehicle (R.O.V.) *VICTOR 6000* on board the R/V *Pourquoi Pas?* during MARSITECruise in 2014. Both push cores were taken about 15 cm apart during dive MRS-DV-596 (Fig. 1). The push core liners are 30 cm in length and 5.5 cm in diameter. MRS-DV5-PC01 with 12.5 cm length was sampled for pore water and sediment analyses while MRS-DV5-PC04 with 8 cm length was subjected to biomarker analyses. After core retrieval from the R.O.V. onboard the R/V *Pourquoi Pas?* the cores were transferred to the cold room at 8°C and immediately processed.

3.2 Pore and bottom water

Pore waters were extracted from push cores using Rhizon samplers (Seeberg-Elverfeldt et al., 2005) connected to pre-evacuated and pre-cleaned 10 ml syringes. Sampling was performed with a depth resolution of 1 cm by inserting the Rhizon samplers through pre-drilled holes into the sediment. The holes were covered with tape during coring. The volume obtained for each sample was transferred into 15 ml HDPE vials. Subsamples for major and minor ion analyses and for determining the isotopic compositions of strontium and calcium were acidified with 15 µl of concentrated HNO_3. All samples were kept refrigerated at 4°C for onshore analyses. Bottom water samples were taken from the supernatant water of the core and filtered with a sterile 0.2 µm Whatman filter.

3.3 Sediment and authigenic carbonates

Sediment samples from MRS-DV5-PC01 were collected immediately after pore water extraction in 1.5 cm slices. Afterwards the depth of the samples was corrected for the sediment volume reduction after pore water extraction. Samples were kept refrigerated at 4°C for onshore analyses. Before further processing, sediments were freeze-dried and authigenic carbonates were then hand-picked. Afterwards, sediments and authigenic carbonates were ground.

3.4 Lipid biomarkers

Sediment samples from MRS-DV5-PC04 (8 cm length) were collected immediately on board in 2 cm slices. All sediment samples were stored at -20°C on board, during ice transport, and on shore before lipid analyses.

4. Methods

4.1 Total alkalinity

Total alkalinity measurements were performed onboard directly after sampling by titration with 0.1 N HCl using a potentiometric titrator (Titrino DMS 716). The pH-meter was regularly calibrated with buffered solutions pH=4 and pH=7. A seawater standard (standard 123) was measured for each set of analyses in order to assess the repeatability of the method. The measurements were performed to pH=4.3 for all samples.

4.2 Major and minor elements

Concentrations of pore water minor elements (Sr^{2+}, Ca^{2+}) were determined by High Resolution Inductively Coupled Plasma Mass-Spectrometry (HR-ICP-MS) and Ion Chromatography (IC), respectively. Sr analyses were carried out with an Element 2 from Thermo Scientific at the Pôle Spectrométrie Ocean (PSO/IUEM). Pore waters were diluted 25-fold with 0.28N nitric acid ULTREX II Ultrapure Reagent (J.T. Baker, Phillipsburg, NJ, USA), in a clean lab. Calibration was done by standard addition using a mono-elemental PlasmaCAL Sr standard (SCP Science, Québec, Canada) and NASS-5 Seawater Reference Material. The overall estimated accuracy was within ± 4% of the Sr molar concentration. Ca analyses were done with a Thermo Scientific ICS-5000 instrument at Ifremer. Pore waters were diluted 500 times on shore and ionic separation was performed with a 2 mm CS-12A column in a flow of metansulfonic acid (MSA). Concentration was calculated using IAPSO (International Association for Physical Sciences of Oceans) Seawater, which was analyzed at the beginning of each run and checked every five samples. The estimated accuracy on the concentration measurements was within ± 3% of the molar concentration.

4.3 Hydrogen sulfide concentration and isotopy

Concentrations of pore water hydrogen sulfide were determined onboard by spectrophotometry as methylene blue complex following the method of Cline (1969). Depending on expected concentrations, 0.1 – 1.2 ml of pore water were subsampled and directly transferred into Eppendorf vials with 100 µl of gelatinous zinc acetate solution to stabilize the sulfide. Different dilutions were prepared (1:1, 1:10, 1:100, 1:200) with oxygen-free water. Subsequently, 100 µl of color reagent (N, N-dimethyl-p-phenylenediamine dihydrochloride solution) and 100 µl of catalyst (Fe(III) solution) were added. After 1 hour, absorbance was measured using a Thermo Scientific Genesys 10uv Scanning spectrophotometer at 670 nm using 1 cm cuvettes.

Sulfide sulfur was released from the gelatinous zinc acetate precipitates as hydrogen sulfide via reaction with acidic chromium chloride solution following Canfield et al. (1986). Hydrogen sulfide was trapped as zinc sulfide in a 3% acetic acid zinc acetate solution and subsequently transferred to silver sulfide via reaction with 0.1 M silver nitrate solution. Precipitates were filtered (<0.45 µm cellulose nitrate filter) and dried at 40 °C.

For sulfur isotope measurements 200 µg of silver sulfide precipitate and 300-600 µg of vanadium pentaoxide (V_2O_5) were homogenously mixed in tin capsules. Isotope analyses were performed with a ThermoFinnigan Delta Plus interfaced to an elemental analyzer.

Results are reported in the standard delta notation ($\delta^{34}S$) as per mil difference to the Vienna Canyon Diablo Troilite (V-CDT) standard.

4.4 Sulfate concentration and sulfur and oxygen isotopes

For sulfate sulfur and oxygen isotope analyses, dissolved sulfate was precipitated as barium sulfate at pH ≤ 2 and sub-boiling conditions using an 8.5% $BaCl_2$ solution following Dogramaci et al. (2001). Precipitates were recovered via filtration (cellulose nitrate membrane filter, pore size 0.45 µm) and dried at 40°C overnight. Sulfate concentrations were determined gravimetrically based on the $BaSO_4$ yield.

For sulfur isotope analyses ($\delta^{34}S$), 200 - 220 µg of barium sulfate precipitate was homogenously mixed with 300 - 600 µg of vanadium pentoxide (V_2O_5) and placed in a tin cup. Isotope measurements were performed in continuous-flow mode via EA-IRMS using a Carlo Erba elemental analyzer interfaced to a ThermoFinnigan Delta Plus isotope ratio mass spectrometer. Results are reported in the standard delta notation as per mil difference to the V-CDT standard. Reproducibility as determined through replicate measurements was generally better than 0.3 ‰. Analytical performance was monitored using international reference materials IAEA S1, S2, S3, NBS 127 and lab reference materials Ag_2S and CdS.

For oxygen isotope analyses ($\delta^{18}O$), 200 - 220 µg of barium sulfate precipitate was placed in a silver cup. Isotope measurements were carried out in continuous-flow mode using a high-temperature combustion unit (TC/EA) interfaced to a ThermoFinnigan Delta Plus XL. Results are reported in the standard delta notation as per mil difference to V-SMOW. Reproducibility as determined through replicate measurements was generally better than 0.5 ‰. International reference materials IAEA SO-5, SO-6, NBS 127 and a lab $BaSO_4$ reference material were measured to monitor analytical performance.

4.5 Carbon isotopic composition of dissolved inorganic carbon

The carbon isotopic composition of dissolved inorganic carbon ($\delta^{13}C_{DIC}$) was measured in a continuous flow-mode using a GasBench-II interfaced to a ThermoFinnigan Delta Plus XL. Briefly, DIC was liberated as CO_2 with phosphoric acid which was subsequently transferred to the mass spectrometer in a helium stream. Water vapor was removed in two nafion water traps.

Results are reported in the standard delta notation as per mil difference to the V-PDB standard. Analytical performance was monitored using a sodium carbonate lab standard. Reproducibility as determined via replicate measurements was generally better than ± 0.2‰.

4.6 Strontium isotopic composition

Authigenic carbonate (aragonite) samples were dissolved in 1N acetic acid (ultrapure). For Sr-separation shrink Teflon columns were filled with 100 µl Sr-spec resin (50 – 100 mm mesh, Eichrom). Each pore water or supernatant sample was loaded in 3N HNO_3, the matrix was washed out in 3N HNO_3 and the strontium washed out with ultra-pure water. Strontium was measured on a Thermo-Fisher TritonTI Thermal Ionization Mass Spectrometer (Institut für Mineralogie, Universität Münster, Germany) in static mode. Aliquots of the samples (300 – 500ng) were loaded with 6N HCl and TaF_5 on tungsten filaments in sandwich technique (c.f., Arning et al., 2009). Mass correction is based on a $^{86}Sr/^{88}Sr$ ratio of 0.1194. Total procedural blanks for strontium were less than 0.1 ng. Repeated runs of NBS standard 987 yielded average $^{87}Sr/^{86}Sr$ ratios of 0.7102087 ±0.000007 (2σ, n=8). The sample data were normalized to a NBS standard 987 value of 0.710248.

4.7 Calcium isotopic composition

For calcium isotope analyses, pore water samples were mixed with a ^{42}Ca-^{43}Ca double-spike (Gussone et al., 2011) to correct for isotope fractionation during ion chromatography and data acquisition in the mass spectrometer. Calcium in the sample was isolated using a 300 ml column volume HCl-chemistry with MCI Gel CK08P, 75–150 µm (Ockert et al., 2013). Of the purified solution, about 300 ng calcium recovered in 2.5 N HCl were loaded on an outgassed Re-single filament with a Ta-activator in sandwich technique. Calcium isotope ratios were determined using a Thermo-Fisher TritonTI Thermal Ionization Mass Spectrometer (Institut für Mineralogie, Universität Münster, Germany). Fractionation correction was carried out using the exponential law and the data reduction follows the description in Heuser et al. (2002). Replicate procedural blank measurements were usually below 1% of total calcium and never exceeded 3%. The calcium isotope values are expressed as $\delta^{44/40}Ca$ values ($\delta^{44/40}Ca$ [‰SRM915a] = (($^{44}Ca/^{40}Ca)_{sample}$/ $^{44}Ca/^{40}Ca)_{standard}$-1) x 1000) relative to SRM915a from the U.S. National Institute of Standards and Technology (NIST). Analyses of IAPSO seawater standard yielded a mean value of 1.87‰ SRM915a with a 2 s.d. of 0.05‰ (n=2). This value lies within the range of previously published values for seawater (1.77 - 2.08 ‰; Tipper et al., 2016). The average 2 s.d. of the samples was determined to be 0.09‰ by replicate measurements.

4.8 U-Th measurements and age calculations

The chemical procedure used in this study followed that described in Bayon et al. (2015). Each sample was dissolved in 7.5 M HNO_3 after addition of a mixed $^{236}U/^{229}Th$ spike, and digested in concentrated HNO_3 on the hotplate. At this stage, sample digestion was incomplete due to the presence of substantial amounts of terrigenous material in the studied samples, typically between 5-8 wt% residues. Because substantial detrital contamination may cause problems for carbonate U-Th dating, these residues were discarded by centrifugation prior to subsequent U-Th chemical purification. U and Th were separated after Fe-oxide co-precipitation using conventional anion exchange techniques. U and Th concentrations and isotope ratios were measured with a MC-ICPMS (Neptune) at the Pôle Spectrométrie Océan (PSO, Ifremer). U-Th carbonate age calculation was performed by the isochron method using the ISOPLOT program (v. 3.71, Ludwig, 2008) in order to correct measured ratios from detrital contamination. The mean isochron age was determined using results obtained for the 4 studied samples and a theoretical end-member at the secular equilibrium (activity ratios = 1.0±0.5). The obtained mean isochron age was given an arbitrary 25% error based on previous estimates (Bayon et al., 2013).

4.9 Total sulfur, total carbon and total inorganic carbon

The abundances of total sulfur (TS), total carbon (TC), and total inorganic carbon (TIC) were measured using a CS-Mat 5500 carbon–sulfur analyzer. Total organic carbon (TOC) abundances were determined as the difference between TC and TIC. Reproducibility was generally better than 5%.

4.10 Organic carbon isotopic composition

Organic carbon isotopic compositions were determined via sealed tube combustion (Strauss et al., 1992). Briefly, freeze dried finely ground sample powder was weighed into quartz tubes that were sealed at one end. Sample powders were decarbonated with 25% HCl, subsequently washed to neutrality using deionized water, and then dried at 40°C in a drying oven for one week. Samples were mixed with 1.5 g CuO, sealed under vacuum and combusted at 850°C for three hours. Liberated CO_2 was cryogenically purified and collected in break-seal tubes. Isotope measurements were performed using a ThermoFinnigan DeltaPlus mass spectrometer at the Institut für Geologie und Paläontologie, Westfälische Wilhelms-Universität Münster, Germany. All values are expressed in the standard δ-notation

relative to the Vienna-Peedee Belemnite Standard (V-PDB) and reported in per mil (‰) relative to V-PDB.

4.11 XRD

The qualitative and semi-quantitative mineralogical composition of the authigenic carbonate samples was analyzed by X-ray diffraction (XRD). Mineralogy was measured on randomly oriented samples using CuKα radiation on a Phillips X'PERT powder diffractometer at the Institut für Mineralogie, Münster, Germany. Scans were run from 20° to 55° 2θ, with a scan rate of 1.5° 2θ/min at 40 kV/30 mA. All of the samples contained some quartz which was used as internal standard. The shift in the d(104) calcite peak was used to determine the Mg content in calcite (Lumsden, 1979).

4.12 Carbon and oxygen isotopic composition

The carbon and oxygen isotopic composition of authigenic carbonates was measured using a Gasbench II coupled to a ThermoFinnigan Delta Plus XL mass spectrometer at the Institut für Geologie und Paläontologie, Münster. At a temperature of 70°C 200 to 300 µg of sample powder were reacted with a 105% phosphoric acid (H_3PO_4) after Wachter and Hayes (1985), liberating carbon dioxide. This was transferred in a stream of helium to the mass spectrometer for isotope measurements. Analytical precision was monitored with three standards (NBS19, IAEA CO-1, IAEA CO-8). Their reproducibility was better than ±0.15‰ for $\delta^{18}O$ and ±0.13‰ for $\delta^{13}C$. All values are given in the standard δ-notation in per mil (‰) relative to the Vienna Peedee Belemnite Standard (V-PDB).

4.13 Lipid biomarker analyses

Freeze-dried sediment samples from core MRS-DV5-PC04 were finely ground and lipids were extracted from ca. 3-5 g of sample with a mixture of dichloromethane:methanol (3:1, v/v) by ultrasonication (3x). Elemental sulfur was removed from total lipid extracts (TLE) by addition of activated copper and stirring samples overnight. An aliquot of the TLE was saponified with 6% KOH in MeOH following the protocol of Elvert et al. (2003). Subsequently, the neutral lipids were extracted (4x) with n-hexane from the basic solution, which was acidified to pH 1 by addition of concentrated HCl; the fatty acids (FAs) were then extracted

(4x) with n-hexane. Neutral lipids were separated into hydrocarbon and alcohol fractions on a solid phase extraction (SPE) silica–NH_2 glass cartridge using previously reported procedures (Hinrichs et al., 2000). FAs were converted to methyl esters (FAMEs) using 14% BF_3 in MeOH. Alcohols were derivatised with N,O-bis(trimethylsilyl)trifluoroacetamide (BSTFA) and pyridine to form trimethylsilyl-(TMS)ethers. Hydrocarbons, alcohols (as TMS-ethers) and fatty acids (as FAMEs) were analyzed by gas chromatography (GC) and gas chromatography-mass spectrometry (GC-MS). Detailed GC and GC-MS conditions are given in Chevalier et al. (2013). Quantification was based on the GC-FID (gas chromatography-flame ionization detector) response of individual peaks relative to known amounts of internal standards (perdeuterated n-tetracosane, androstanol, heneicosanol and nonadecanoic acid). Compound-specific stable carbon isotope composition ($\delta^{13}C$) was determined, at interval depth for each fraction where concentrations are maximum, by isotope ratio monitoring-gas chromatography-mass spectrometry (IRM-GC-MS) using a ThermoFinnigan Delta Plus XL instrument. The GC was a ThermoFinnigan Trace GC, and the analytical conditions were identical as those for GC and GC-MS. $\delta^{13}C$ values are in the δ notation relative to the VPDB standard, and reported in ‰. All values have been corrected for the addition of carbon during derivatization, and have an analytical standard deviation of less than ±1.0‰.

5. Results

5.1 Pore and bottom water geochemistry

Pore water alkalinity is generally increasing with depth towards values around 26 mol/l (Table 1). The sulfate concentration is showing an opposite trend with decreasing values down to about 1.2 mmol/l. The corresponding sulfide profile exhibits values around 1 mmol/l at the top and bottom of the core and a maximum concentration of 2 mmol/l between 4.5 and 10.5 cm. Both Sr^{2+} and Ca^{2+} concentrations show a distinct decrease in the first pore water sample at 1.5 cm relative to seawater with 65.1 µmol/l (seawater: 91 µmol/l) and 8.1 mmol/l (seawater: 10.3 mmol/l), respectively. The depth profile of the Sr^{2+} concentration shows little variation while the Ca^{2+} concentration exhibits a distinct decrease to a minimum value of about 5 mmol/l.

Sulfate sulfur has a seawater-like isotopic composition in the bottom water (+20.8 ‰) but varies around +30 ‰ in the pore water throughout the core including a low value (+27.5 ‰) at the bottom of the core (Table 1, Fig. 4). The oxygen isotopic composition of sulfate

parallels the sulfate sulfur isotope depth trend (Table 1). Because of low sulfide concentrations, samples for sulfur isotopic composition of sulfide were pooled. The three values indicate a positive trend from top to bottom of the core from negative (-8.9 ‰) to a slightly positive value of +1.9 ‰ (Table 1, Fig. 4).

The carbon isotopic composition of the dissolved inorganic carbon is starting with seawater-like values (-1.7 ‰) at the top of the core and decreases towards lighter values with depth up to about -32 ‰ with the exception of a positive excursion at 8.5 cm with about -14 ‰ (Table 1). The calcium isotopic composition of bottom water is slightly elevated (2.03 ‰) with respect to normal seawater (1.89 ‰; Tipper et al., 2016). The downcore values are similar to bottom water and range between 2.08 and 2.16 ‰ (Table 1). Only the two lowermost samples show slightly elevated values with up to 2.26 ‰. The Sr isotopic composition of the bottom water is seawater-like and shows a trend towards slightly more radiogenic values with depth from 0.709173 to 0.709190.

5.2 Sediment and authigenic carbonate geochemistry

The depth of the sediment samples differs slightly from the pore water samples because during pore water sampling of the core, the sediment dewatered involving a volume reduction. The TC, TOC and TIC values of the sediments have to be treated with caution because macroscopic authigenic carbonates were subsampled before sediment analysis. Consequently, these values rather reflect the fine-grained sediments (smaller than sand-size). While authigenic carbonates were found at all depth intervals in the core, a change in mineralogy and habit can be observed. The upper about 7 cm of the core are dominated by thin crusts composed of pure aragonite (Table 2). This core interval is characterized by a slightly higher TIC content in the fine fraction, and low TS and TOC contents between 2 and 4 wt.%. The isotopic composition of the sedimentary organic matter shows extremely light values in the shallowest part with about -61 ‰ while values increase with depth to -26 ‰ (Table 2).

Below 8 cm in the core, authigenic carbonates show a mixed mineralogy with aragonite dominating over high-Mg calcite (20-21 Mol% $MgCO_3$) or vice versa (Table 2). The habit is mostly nodular. The carbon isotopic composition of all authigenic carbonates varies between -28 and -33 ‰ (Table 2). The oxygen isotopic composition is between 1.4 and 3.38 ‰ (Table 2). Ca isotope ratios were only measured on pure aragonitic samples. The $\delta^{44/40}Ca$ values vary from 0.64 to 0.93 ‰ with the highest value at the bottom of the core (Table 2). The $^{87}Sr/^{86}Sr$ values of the same set of samples used for Ca isotopes show values ranging between 0.709184 and 0.709192 (Table 2).

5.3 Lipid Biomarkers

Sediment samples from push core MRS-DV5-PC04 (8 cm depth) contained high amounts of isoprenoid glycerol diethers of archaeal origin, namely archaeol (2,3-di-O-phytanyl-sn-glycerol) and sn-2-hydroxyarchaeol (Koga et al., 1998) (Fig. 5b). The concentrations reached up to 26.1 µg/g dry weight (dw) with sn-2-hydroxyarchaeol being predominant at the 2-4 cm interval sediment depth (Table 3). The irregular isoprenoid hydrocarbons (Elvert et al., 2000, and references therein), crocetane (2,6,11,15-tetramethylhexadecane) and PMIs (2,6,10,15,19-pentamethylicosenes; polyunsaturated irregular C_{25} isoprenoid alkenes with 1 to 4 unsaturations) were further important archaeal lipids (Fig. 5a), with concentrations up to 0.82 µg/g dw and 4.68 µg/g dw, respectively (Table 3). At interval sediment depth where concentrations are maximum, archaeal glycerol diethers and isoprenoid hydrocarbons were strongly depleted in ^{13}C with $\delta^{13}C$ values as low as -114 ‰ (Table 3).

Among the bacterial lipids, substantial amounts of fatty acids indicative of sulfate reducing bacteria were detected (Fig. 5c), such as iso- and anteiso-$C_{15:0}$ (i-, ai-C_{15}), $C_{16:1\omega5}$, Me-C_{16} and cy$C_{17:0\omega5,6}$ (Niemann and Elvert, 2008, and references therein). The *i*- and *ai*-$C_{15:0}$ concentrations were between 4.20 µg/g and 14.1 µg/g dw, respectively (Table 3). $C_{16:1\omega5}$, Me-C_{16} and cy$C_{17:0\omega5,6}$ occurred at up to 43.3 µg/g dw. At the 2-4 cm interval sediment depth, bacterial FAs assigned to SRB were ^{13}C-depleted with $\delta^{13}C$ values ranging from -95 ‰ to -86 ‰, albeit enriched by 20 ‰ relative to archaeal lipids (Table 3).

6. Discussion

6.1 Sulfate-driven anaerobic oxidation of methane

The downcore decrease in pore water sulfate concentration and a parallel increase in sulfate sulfur isotopic composition from a seawater-like value of +20.8 ‰ for the bottom water to more positive, i.e. ^{34}S-enriched values, at depth indicates progressive microbial reduction of sulfate (e.g., Canfield, 2001). Support for this stems from a parallel increase in $\delta^{18}O_{SO4}$, again from seawater-like value of +8.7 ‰ to an ^{18}O-enriched value of +17.5 ‰. In fact, both isotopes exhibit a clear linear correlation (r^2=0.92) (Fig. 6).

In the marine realm, remineralization of sedimentary organic matter proceeds via a sequence of microbially driven redox reactions (e.g., Froelich et al., 1979; Canfield and Thamdrup, 2009), with aerobic respiration being followed downwards in the anoxic part of the sedimentary column by organoclastic sulfate reduction (OSR):

$$2\ CH_2O + SO_4^{2-} \rightarrow H_2S + 2\ HCO_3^-$$

Sulfate, serving as the terminal electron acceptor, is derived from pore water. Progressive sulfate reduction results in a progressing depletion of pore water sulfate concentration, if sulfate reduction exceeds sulfate replenishment. Resulting hydrogen sulfide is commonly scavenged by iron and ultimately precipitates pyrite, whereas resulting bicarbonate forms diagenetic calcium carbonate, thereby cementing the pore space.

Microbial sulfate reduction is associated with a strong kinetic isotope effect. Sulfate reducing bacteria preferentially reduce the $^{32}SO_4$ resulting in ^{32}S-enriched hydrogen sulfide. A range in sulfur isotopic fractionation of 20-40 ‰ between parental sulfate and resulting hydrogen sulfide is commonly observed in natural settings (e.g., Canfield, 2001), but maximum values of 60-70 ‰ have been measured in nature and confirmed by experimental work (Sim et al., 2011; Wortmann et al., 2001). With ^{32}S-enriched hydrogen sulfide being scavenged by iron and precipitated as ^{32}S-enriched sedimentary iron sulfide, the progressively depleting residual pore water exhibits a unidirectional Rayleigh-type enrichment in ^{34}S towards more positive $\delta^{34}S_{SO4}$ values.

In addition to OSR, sulfate reduction can be coupled to the oxidation of methane, a paired reaction termed sulfate-driven anaerobic oxidation of methane (AOM):

$$CH_4 + SO_4^{2-} \rightarrow HS^- + HCO_3^- + H_2O$$

Below the zone of sulfate reduction, microbial remineralization of sedimentary organic matter continues via methanogenesis. Resulting biogenic methane diffuses upwards through the sedimentary column where it can be utilized by sulfate reducing bacteria as electron donor. The respective paired reaction, i.e. sulfate driven anaerobic oxidation of methane, consumes both upwards diffusing methane and pore water sulfate, defining the so called sulfate-methane transition zone (SMTZ). Pore waters in the SMTZ exhibit a near-linear downward decrease in sulfate concentration and an upward decrease in methane concentration (e.g., Borowski et al., 1996). Rapid and frequently near quantitative consumption of sulfate results in a strong ^{34}S-enrichment of the residual dissolved sulfate. Moreover, iron sulfide precipitates also display a ^{34}S-enriched sulfur isotopic signature (e.g., Peketi et al., 2012; Lin et al., 2016; 2017). Similarly diagnostic carbon isotope signatures characterize authigenic carbonates that form via AOM (see below).

The sulfur isotopic composition of pore water sulfate from push core MRS-DV5-PC01 displays a range in $\delta^{34}S$ values between +27.5 and +35.9 ‰ over the entire depth interval (Fig. 4) that is distinctly different from the seawater-like value of +20.8 ‰ for sulfate in the bottom water at the site of the shallow push core MRS-DV5-PC01. Three samples of pore water sulfide, pooled over depth intervals of 2-4 cm, are depleted in ^{34}S compared to the

parental sulfate. Samples from the two shallow intervals are depleted by as much as 40 ‰ and in the deepest interval by around 25 ‰. In addition, the sulfate sulfur and sulfate oxygen isotopic compositions correlate well (Fig. 6). A calculated slope of 0.55 is above the slope range of 0.24-0.4 of Antler et al. (2015) that was defined as characteristic for AOM with "methane in excess", i.e. free methane bubbling out of the sediment as typical for cold seep areas (e.g., Judd and Hovland, 2007; Solomon et al., 2009; Suess et al., 1999). A similar observation was made by Feng et al. (2016). They also investigated a site with AOM at shallow sediment depth. Their slope of 0.53 indicated, although methane was available in excess, a rather "methane diffusion-limited" environment after Antler et al. (2015). The study of Feng et al. (2016) and our results indicate that these discrepant observation require further investigation.

In the nearby sediment core (MRS-DV5-PC04), the detection of diagnostic archaeal lipids of anaerobic methane oxidizers (isoprenoid alkanes and alcohols) and specific bacterial lipids of sulfate-reducers (fatty acids) detected with strong ^{13}C-depletions (-86 ‰ to -114 ‰) indicate that AOM activity occurs in association with bacterial sulfate reduction in the upper few centimeters of the seafloor. Moreover, available data from methane-rich environments allow us to distinguish dominant AOM assemblages on the basis of specific lipid patterns (for a review see Niemann and Elvert (2008)). Accordingly, the predominance of sn-2-hydroxyarchaeol over archaeol (ratio 1.9), together with the presence of crocetane, are consistent with a dominance of ANME-2 archaea within the microbial community. The same ANME community was detected at this location by Chevalier et al. (2013). The presence of ^{13}C-depleted cyC17:0 FA, as well as the low ratio of ai-C15:0 relative to i-C15:0 (between 1.2 and 1.6) typify SRB eco-types from the Desulfosarcina/Desulfococcus (DSS) cluster that have been found in association with ANME-2 archaea (Niemann and Elvert, 2008 and references therein).

In summary, bacterial lipids, sulfate sulfur and oxygen isotope data clearly indicate microbial sulfate reduction. A positive correlation between sulfate sulfur and oxygen isotope data with a slope of 0.55 as well as ^{13}C-depleted microbial lipids strongly suggests sulfate-driven anaerobic oxidation of methane. Further evidence is provided by authigenic carbonates and their geochemical and isotopic characteristics.

6.2 Controls on authigenic carbonate formation

6.2.1 Carbon source and formation process

The carbon isotopic signature of carbonates provides important information about the carbon source and therefore also on the process of authigenic carbonate formation. In core MRS-

DV5-PC01, abundant carbonates (Fig. 3) were found in each sediment sample (1.5 cm interval). The $\delta^{13}C$ values of all these samples show a narrow range from -27.69 to -33.40 ‰ (Table 2, Figs. 7, 8). No clear depth trend is discernible except that the two samples with the lowest values are found at the bottom of the core (Fig. 7). The analyses of hydrocarbon gas in the Çinarcik Basin has shown that it is mainly composed of biogenic methane (99.74 %) with an isotopic signature of $\delta^{13}C_{methane}$ between -62.1 and -63.8 ‰ (Ruffine et al., this issue). Authigenic carbonates precipitate from the dissolved inorganic carbon (DIC) in the pore water which might be a mixture of different sources like e.g. seawater dissolved inorganic carbon, marine/terrestrial organic matter, methane. Therefore, the isotopic composition of the DIC identifies the process responsible for carbonate formation. One carbon source, biogenic methane, has already been identified in the Çinarcik Basin (Ruffine et al., this issue). Its typical isotopic composition ranges between -50 and -110 ‰ (Whiticar, 1999). Other carbon sources may be the dissolved inorganic carbon from seawater ($\delta^{13}C$ ~ 0‰) or marine organic matter (about -17 to -22 ‰). The $\delta^{13}C$ values of the DIC of MRS-DV5-PC01 are variable and decrease from -1.68 to -31.67 ‰ (Table 1, Fig. 7). The value in the shallowest sample at 1.5 cm depth shows a seawater-like signature probably due to intensive mixing of seawater and pore water in the fluffy layer. The steady decrease with depth to a value as low as -31.67 ‰ indicates that a carbon source depleted in ^{13}C is becoming more prominent. Organic matter can be excluded since the $\delta^{13}C$ values are lighter than typical marine organic matter (see above). Instead, the strongly ^{13}C depleted carbon isotope values down to -31.67 ‰ suggest methane to become the main carbon source. These results therefore support the idea that authigenic carbonate precipitation was induced by a strong increase in alkalinity (Table 1) due to AOM. The AOM activity is also confirmed by the presence of ANME-2 biomass in the nearby sediment core MRS-DV5-PC04 revealed by specific ^{13}C-depleted archaeal lipids, which is consistent with the study of Chevalier et al. (2013).

Because of negligible fractionation of carbon isotopes during incorporation into authigenic carbonate, a recently precipitated carbonate is characterized by a $\delta^{13}C$ value that matches the $\delta^{13}C$ value of the DIC of the pore water. When comparing the $\delta^{13}C$ values from DIC and from authigenic carbonates (Fig. 7), it becomes evident that only at the bottom of the core carbonates are currently forming. The maximum in alkalinity (Table 1), the decrease in sulfate concentration and high $\delta^{34}S_{SO4}$ values (Fig. 4) as well as lipid biomarker evidence in MRS-DV5-PC04 collectively point to a shallow sulfate-methane transition zone (SMTZ) around 12 cm sediment depth where AOM is the main process inducing the precipitation of authigenic carbonates.

Additional support comes from the Sr isotopic composition of carbonates and pore waters. The strontium isotopic signature is archived in carbonates during their growth without isotopic

fractionation compared to ambient water and have been used in the past to reconstruct the formation depth of authigenic carbonates (Meister et al., 2007; Teichert et al., 2009). The lowest carbonate sample at 12 cm depth mirrors the pore water isotopic composition within error (Fig. 9A). This is not the case for the shallower samples and provides strong evidence for current authigenic carbonate precipitation at the proposed SMTZ.

Support comes also from the Ca isotopic composition of pore waters and carbonates. During carbonate precipitation we expect to see a strong decrease in Ca concentration together with increasing $\delta^{44/40}$Ca values (Teichert et al., 2009). The measured bottom water Ca isotopic composition is slightly elevated (2.03 ‰, Table 1) with respect to previously published seawater values (~ 1.89 ‰, Tipper et al., 2016). Although we could expect to see the influence of the riverine input into the SoM, this is not the case. The Ca isotopic composition of rivers is distinctly lighter as seawater (0.67 - 1.25 ‰; Tipper et al., 2016). Although there is very sparse data yet for the Sea of Marmara, we can speculate that the pore water represents a source of a rather heavy $\delta^{44/40}$Ca that is being released to the bottom water of the SoM. In the upper 10 cm of the sediments, the $\delta^{44/40}$Ca scatters around a mean value of 2.12 ‰. Then, Ca concentrations decrease to about half the seawater concentration combined with an increase in $\delta^{44/40}$Ca of 0.23 ‰. The strong decrease in Ca concentration in shallow marine sediments has commonly been attributed to authigenic carbonate formation (e.g. Teichert et al., 2009; Wallmann et al., 1997). Previous studies have shown that heavy Ca isotopes are depleted in carbonates relative to the fluid (e.g. Gussone et al., 2005; 2003; Lemarchand et al., 2004; Marriot et al., 2004). A Ca isotopic composition heavier than seawater in the pore water is therefore consistent with carbonate formation. Experimental studies on inorganic aragonite have provided fractionation factors for specific temperatures (Gussone et al., 2003). For a bottom water temperature of 14.5 °C we would expect a 1000lnα of about -1.7 ‰ ($\delta^{44/40}Ca_{carbonate}$ = 0.56 ‰). The carbonate at 12 cm depth has, however, a higher $\delta^{44/40}$Ca of 0.93 ‰, which is 0.37 ‰ heavier than expected (Table 2). This observation cannot be explained with a Raleigh-type fractionation during precipitation because the $\Delta^{44/40}Ca_{aragonite\text{-}fluid}$ will increase during ongoing precipitation. There might however be other factors leading to a decrease in the fractionation factor like precipitation rate, stoichiometry (Ca : CO_3) and supersaturation (Lemarchand et al., 2004; Nielsen et al, 2013; 2012; Tang et al., 2008). In a similar environment, in the presence of gas hydrates at Hydrate Ridge (Oregon, USA), the same observation of a reduced fractionation factor for aragonite has been made. Authigenic aragonite, precipitated due to AOM in the shallow subsurface, has shown $\delta^{44/40}Ca_{carbonate}$ values 0.35 - 0.74 ‰ heavier as expected (Teichert et al., 2005). It is however not possible to differentiate if this observation is a coincidence or attributed to e.g. high precipitation rates and/or supersaturation in AOM dominated environments.

6.3 Indicators for a paleo-SMTZ close to the seafloor

Based on pore water and carbonate data, the current SMTZ at MRS-DV5-PC01 is starting at about 11 cm depth and probably extends down to a little further than 12.5 cm depth which is the length of the core (Fig. 4). Compared to many other world-wide methane seep sites, this is a very shallow SMTZ depth (e.g. Borowski et al., 1996; Kastner et al., 2008; Yoshinaga et al., 2014). However, there are indications that in the past the SMTZ was located even shallower within the sedimentary column. Possible evidence for the presence of paleo-SMTZ's comes from authigenic carbonates which can serve as archives for past seepage events (e.g. Bayon et al., 2013; Teichert et al., 2014; 2003). The carbonates found in the upper about 10 cm of core MRS-DV5-PC01 (Fig. 7) have not been precipitated from today's pore waters. This means they are older than the carbonates precipitated at the current SMTZ. A first age approximation are sedimentation rates. In Çinarcik Basin, Çağatay et al. (2004) have presented an approximate sedimentation rate of 1.9 mm/yr. Armijo et al. (2005) give a range for the deep basin part of 1-3 mm/yr. According to these sedimentation rates, the sediments of MRS-DV5-PC01 would have been deposited within less than 42-125 years. This is a rough approximation since we do not have sedimentation rates of the coring location which is at the SE border of the deep basin part (Fig. 1). Additional age information comes from U-Th dating of 4 pure aragonite samples (Table 4). Due to the high detrital content of ^{232}Th and the young age of the samples it was unfortunately not possible to derive reliable ages for each sample. Yet it was possible to derive an isochron age by considering the 4 samples together. The mean age of 235 ± 60 yr B.P. is somewhat higher than the estimated ages from the sedimentation rates. Still, this shows that in the very recent past the SMTZ was almost right at the seafloor and methane emanation rates were most probably higher than during the time of sampling.

The proposed paleo-SMTZ almost right at the seafloor is also supported by the mineralogical composition of the authigenic carbonates. In the upper 8 cm, authigenic carbonates are composed of pure aragonite (Fig. 7, Table 2). Aragonite has been shown to precipitate preferentially in the presence of sulfate and high Mg^{2+}/Ca^{2+} ratios (Burton, 1993). Such an environment is found close to the seafloor. At low sulfate concentrations calcite is favored over aragonite (Burton, 1993). The HMC component of the samples below 8 cm depth might therefore represent deeper precipitates relative to the aragonites. These HMC samples are high in Mg and have 20-21 Mol% $MgCO_3$ which is typical for methane seeps and often found near the seafloor (e.g. Gieskes et al., 2005; Naehr et al., 2007; Peckmann and Thiel, 2004; Teichert et al., 2014; 2005). Often, the HMC occurs also in paragenesis with aragonite (Crémière et al., 2012).

Supporting a very near seafloor precipitation is the oxygen isotopic composition of the carbonates. The aragonites show $\delta^{18}O$ values close to the calculated equilibrium value after Grossman and Ku (1986) of 2.80 ‰ with a bottom water temperature of 14.5 °C and a $\delta^{18}O$ for bottom water of 1.6 ‰ (Fig. 8; Aloisi et al., 2015). Since the samples are very young we assume no major changes in these two parameters over time. All aragonites are however between 0.2 and 0.3 ‰ lighter than the equilibrium value (Fig. 8). Crémière et al. (2012) made the same observation on samples from the Çinarcik Basin and interpreted this as possible influence from brackish waters from below. We see, however, no evidence for the influence of brackish waters at this depth (12.5 cm core length). Possibly a slightly elevated temperature of 1°C would fit with the measured values or a pore water isotopic composition that slightly deviates from the bottom water (1.4 ‰). Since we do not have in situ measurements of these two parameters we cannot differentiate between the influence of temperature or pore water composition. For the carbonate samples with HMC, either with HMC as main component and aragonite as minor component and vice versa, the picture is similar. Oxygen isotope equilibrium values calculated after Anderson and Arthur (1983) and Kim and O'Neil (1997), both corrected for the amount of Mol% $MgCO_3$ (Tarutani et al., 1969), give a $\delta^{18}O$ of 3.17 ‰ and 2.86 ‰, respectively (Fig. 8). These values show that the equilibrium values span a wide range depending on which formula is used. The value by Anderson and Arthur (1983) fits the HMC-dominated samples quite well while the aragonite-dominated samples are closer to the equilibrium value for aragonite (Fig. 8). A calculated equilibrium value following Kim and O'Neil (1997) does not fit the HMC-dominated sample very well (Fig. 8). It therefore remains difficult to clearly interpret the oxygen isotope data of the HMC-bearing samples.

6.4 Conceptual model of a highly dynamic methane bubbling site

The study location in the Çinarcik Basin shows a complex picture of methane seepage activity preserved in the studied push cores. Based on overall sedimentation rates for Çinarcik Basin, the sediments span a time frame from 42 to 125 years (Armijo et al., 2005; Çağatay et al., 2004) and based on our U-Th dating from 175 to 295 years. There is no overlap but since we do not have precise sedimentation rates for the studied location, the sedimentation rates can only be regarded as a rough estimate. The U-Th ages should be regarded as more reliable. Support comes also from a nearby Calypso core (N 40°42.977194, E 29°06.703129) of 10 m length. From onboard core description (pers. com. M.M. Blanc-Valleron) the transition from marine to lacustrine sediments starts at 6 m depth. Based on our sedimentation rates from U-Th dating (0.5 mm/yr) the transition that started about 12.000 years ago (Vidal et al., 2010) corresponds to a sediment depth of 6 m.

With a shallow SMTZ around 12 cm depth this site can be regarded as a very active methane seepage locality. This conclusion is supported by the observation of methane bubbling out of the sediment and polychaetes growing at the seafloor (Fig. 2, 3). Further evidence is provided by authigenic carbonate precipitation (Fig. 3), the presence of clams in the sediments as well as a microbial mat in the upper ca. 4 cm of the sediments (Table 2) showing highly negative $\delta^{13}C$ values of the organic matter (-61 ‰). Still, the presence of ^{13}C-depleted authigenic carbonates in the sediments above the SMTZ shows that the SMTZ has been even shallower in the past, and evidence of variable methane flux. This or these rather fast shifts in the SMTZ depth over time make it extremely difficult to reconstruct the chronology of carbonate precipitation in the sediments. It is possible that the SMTZ shifts up and down in an oscillatory way. Indeed, the area is characterized by high seismic activities. It has been suggested that such events are responsible for the change of methane flux within the sedimentary column, and accordingly in fluctuations of the SMTZ (Ruffine et al., 2015).

This means that carbonates may have precipitated e.g. in the order: 10 cm, 40 cm, 20 cm. It is important to keep this in mind when looking at MRS-DV5-PC01 with carbonates in all depth intervals. Very likely, the present depth order is not a chronological order. Unfortunately, it is not possible to reconstruct all the details because of the short time scale involved and limited dating possibilities. The available dataset is also not consistent enough to constrain this reconstruction by modeling neither.

Considering all data, we propose the following scenario. Methane seepage and authigenic carbonate formation have been active at this location for at least the last 175 to 295 years B.P. This time span coincides with two major earthquakes 1766 (M~7) and 1754 in Çinarcik Basin (Ambraseys and Jackson, 2000) that potentially triggered the increased seepage of methane (Fig. 10). Of importance might have also been the 1894 Yalova (M~7) earthquake which most probably produced a large fault at the southern edge of Çinarcik Basin south of the study site (Armijo et al., 2005). If this earthquake initiated or enhanced methane seepage at the MRS-DV5-PC01/PC04 location can only be speculated. In the following years, the SMTZ might have frequently shifted up and down leading to authigenic carbonate precipitation at various depths. The most recent carbonates seem to be located at about 1 cm depth. This corresponds to an age of about 10 years based on the slow sedimentation rates. This implies that the SMTZ has shifted downwards about 10 years ago from a position basically at the seafloor to now about 12 cm depth.

Conclusions

A high resolution multi-proxy study was conducted for two short sediment push cores from the SE Çinarcik Basin in an active methane bubbling area. Results provide insight into the dynamics of methane seepage and microbial communities and the connected biogeochemical responses. Both cores show a complex history of methane seepage in a short time span. The major conclusions of our study are:

1) A steep sulfate gradient together with the presence of ANME-2 biomass revealed by specific ^{13}C-depleted archaeal lipids show that methane is rising by advection at the studied location.

2) The results indicate that slight fluctuations up and down (cm-scale) in the depth of the SMTZ can happen over short time scales (ca. 200 years). These fluctuations are most probably related to changes in methane emanation which might be coupled to earthquake activity or the fault movement such as ground shaking.

3) The deposits of seeps have to be investigated with great care regarding chronology. When looking at authigenic precipitates the law of superposition is not necessarily valid.

Acknowledgements

The captain and the crew of the R/V Pourquoi Pas? as well as the scientific party of the MARSITECruise expedition are warmly thanked for their support at sea. We thank A. Fugmann and A. Lutter (Westfälische Wilhelms-Universität Münster) for their assistance in the laboratory. We greatly appreciate the editorial handling of N. Çağatay as well as the reviews of an anonymous reviewer and of Tobias Himmler who helped to strengthen and improve the manuscript.

References

Aloisi, G., Soulet, G., Henry, P., Wallmann, K., Sauvestre, R., Vallet-Coulomb, C., Lécuyer, C., Bard, E., 2015. Freshening of the Marmara Sea prior to its post-glacial reconnection to the Mediterranean Sea. Earth Planet. Sci. 413, 176-185.

Anderson, T.F., Arthur, M.A., 1983. Stable isotopes of oxygen and carbon and their application to sedimentologic and paleoenvironmental problems. - in: M.A. Arthur (ed.) Stable Isotopes in Sedimentary Geology, 1-1 to 1-151, SEPM short course, No. 10, Dallas.

Ambraseys, N.N., Jackson, J.A., 2000. Seismicity of the Sea of Marmara (Turkey) since 1500. Geophys. J. Int. 141(3), F1-F6

Antler, G., Turchyn, A.V., Herut, B., Sivan, O., 2015. A unique isotopic fingerprint of sulfate-driven anaerobic oxidation of methane. Geology 43, 619-622.

Armijo, R., Pondard, N., Meyer, B., Ucarkus, G., Mercier de Lépinay, B., Malavieille, J., Dominguez, S., Gustcher, M.-A., Schmidt, S., Beck, C., Cagatay, N., Cakir, Z., Imren , C., Eris, K., Natalin, B., Özalaybey, S., Tolun, L., Lefèvre, I., Seeber, L., Gasperini, L., Rangin, C., Emre, O., Sarikavak, K., 2005. Submarine fault scarps in the Sea of Marmara pull-apart (North Anatolian Fault): Implications for seismic hazard in Istanbul. Geochem. Geophy. Geosy., 6, Q06009, doi:10.1029/2004GC000896.

Bayon, G., Henderson, G.M., Etoubleau, J., Caprais, J.-C., Ruffine, L., Marsset, T., Dennielou, B., Cauquil, E., Voisset, M., Sultan, N., 2015. U-Th isotope constraints on gas hydrate and pockmark dynamics at the Niger Delta margin. Mar. Geol. 370, 87-98.

Bayrakci, G., Scalabrin, C., Dupré, S., Leblond, I., Tary, J.B., Lanteri, N., Augustin, J.M., Berger, L., Cros, E., Ogor, A., Tsabaris, C., Lescanne, M., Géli, L., 2014. Acoustic monitoring of gas emissions from the seafloor. Part II: a case study from the Sea of Marmara. Mar. Geophys. Res. 35, 211-229.

Bayon, G., Dupré, S., Ponzevera, E., Etoubleau, J., Chéron, S., Pierre, C., Mascle, J., Boetius, A., de Lange, G., 2013. Formation of carbonate chimneys in the Mediterranean Sea linked to deepwater oxygen depletion. Nat. Geosci., 6, 755-760.

Borowski, W.S., Paull, C.K., Ussler, I.I.I.W., 1996. Marine pore-water sulfate profiles indicate in situ methane flux from underlying gas hydrate. Geology 24, 655-658.

Bourry, C., Chazallon, B., Charlou, J.L., Donval, J.P., Ruffine, L., Henry, P., Geli, L., Çağatay, M.N., Inan, S., Moreau, M., 2009. Free gas and gas hydrates from the Sea of Marmara, Turkey Chemical and structural characterization. Chem. Geol. 264, 197-206.

Burton, E.A., 1993. Controls on marine carbonate cement mineralogy: review and reassessment. Chem. Geol. 105, 163-179.

Çağatay, M.N., Özcan, M., Güngör, E., 2004. Pore-water and sediment geochemistry in the Marmara Sea (Turkey): early diagenesis and diffusive fluxes. Geochem.-Explor. Env. A. 4, 213-225.

Çağatay, M.N., Yildiz, G., Bayon, G., Ruffine, L., Henry, P., this issue. Seafloor authigenic carbonate crusts along the submerged part of the North Anatolian Fault in the Sea of Marmara: Mineralogy, geochemistry, textures and genesis. Deep-Sea Res. Pt. II

Canfield, D.E., Raiswell, R., Westrich, J.T., Reaves, C.M., Berner, R.A., 1986. The use of chromium reduction in the analysis of reduced inorganic sulfur in sediments and shales. Chem. Geol. 54, 149-155.

Canfield, D.E., 2001. Isotope fractionation by natural populations of sulfate-reducingbacteria. Geochim. Cosmochim. Acta 65, 1117-1124.

Canfield, D.E., Thamdrup, B., 2009. Towards a consistent classification scheme for geochemical environments, or, why we wish the term suboxic' would go away. Geobiology 7, 385-392.

Chevalier, N., Bouloubassi, I., Birgel, D., Taphanel, M.H., López-García, P., 2013. Microbial methane turnover at Marmara Sea cold seeps: A combined 16SrRNA and lipid biomarker investigation. Geobiology 11, 55-71.

Chevalier, N., Bouloubassi, I., Birgel, D., Crémière, A., Taphanel, M.-H., Pierre, C., 2011. Authigenic carbonates at cold seeps in the Marmara Sea (Turkey): A lipid biomarker and stable carbon and oxygen isotope investigation. Mar. Geol. 288, 112-121.

Cline, J.D., 1969. Spectrophotometric determination of hydrogen sulfide in natural waters. Limnol. Oceanogr. 14(3), 454-458.

Crémière, A., Bayon, G., Ponzevera, E., Pierre, C., 2013. Paleo-environmental controls on cold seep carbonate authigenesis in the Sea of Marmara. Earth Planet. Sci. 376, 200-211.

Crémière, A., Pierre, C., Blanc-Valleron, M.-M., Zitter, T., Çağatay, M.N., Henry, P., 2012. Methane-derived authigenic carbonates along the North Anatolian fault system in the Sea of Marmara (Turkey). Deep-Sea Res. Pt. I 66, 114-130.

Dogramaci, S.S., Herczeg, A.L., Schiff, S.L., Bone, Y., 2001. Controls on $\delta^{34}S$ and $\delta^{18}O$ of dissolved SO_4 in aquifers of the Murray Basin, Australia and their use as indicators of flow processes. Appl. Geochem. 16, 475-488.

Dupré, S., C. Scalabrin, C. Grall, J.-M. Augustin, P. Henry, A. M. C. Şengör, N. Görür, M. N. Çağatay, and L. Géli, 2015. Tectonic and sedimentary controls on widespread gas missions in the Sea of Marmara: Results from systematic, shipborne multibeam echo sounder water column imaging. J. Geophys. Res.-Sol. Ea. 120, 2891-2912.

Elvert, M., Boetius, A., Knittel, K., Jorgensen, B. B., 2003. Characterization of specific membrane fatty acids as chemotaxonomic markers for sulfate-reducing bacteria involved in anaerobic oxidation of methane. Geomicrobiol. J. 20, 403-419.

Elvert, M., Suess, E., Greinert, J., Whiticar, M.J., 2000. Archaea mediating anaerobic methane oxidation in deep-sea sediments at cold seeps of the eastern Aleutian subduction zone. Org. Geochem. 31, 1175–1187.

Feng, D., Peng, Y., Bao, H., Peckmann, J., Roberts, H.H., Chen, D., 2016. A carbonate-based proxy for sulfate-driven anaerobic oxidation of methane. Geology 44(12), 999-1002.

Froelich, P.N., Klinkhammer, G.P., Bender, M.L., Luedtke, N.A., Heath, G.R., Cullen, D., Dauphin, P., Hammond, D., Hartman, B., Maynard, V., 1979. Early oxidation of organic matter in pelagic sediments of the eastern equatorial Atlantic: suboxic diagenesis. Geochim. Cosmochim. Acta 43, 1075-1090.

Géli, L., Henry, P., Zitter, T., Dupré, S., Tryon, M., Çağatay, M.N., de Lépinay, B.M., Le Pichon, X., Şengör, A.M.C., Görür, N., Natalin, B., Uçarkuş, G., Özeren, S., Volker, D., Gasperini, L., Burnard, P., Bourlange, S., the Marnaut Scientific Party, 2008. Gas emissions and active tectonics within the submerged section of the North Anatolian Fault zone in the Sea of Marmara. Earth Planet. Sci. Lett. 274, 34–39.

Gieskes, J., Mahn, C., Day, S., Martin, J.B., Greinert, J., Rathburn, T., McAdoo, B., 2005. A study of the chemistry of pore fluids and authigenic carbonates in methane seep environments: Kodiak Trench, Hydrate Ridge, Monterey Bay, and Eel River Basin. Chem. Geol. 220, 329-345.

Grall, C., Henry, P., Tezcan, D., Mercier de Lepinay, B., Bécel, A., Géli, L., Rudkiewicz, J.-L., Zitter, T., Harmegnies, F., 2012.Heat flow in the Sea of Marmara Central Basin: Possible implications for the tectonic evolution of the North Anatolian fault. Geology 40(1), 3-6.

Grossman, E.L., Ku, T.L., 1986. Oxygen and carbon isotope fractionation in biogenic aragonite: temperature effects. Chem. Geol. 59, 59-74

Gussone, N., Nehrke, G., Teichert, B.M.A., 2011. Calcium isotope fractionation in ikaite and vaterite. Chem. Geol. 285, 194-202.

Gussone, N., Hönisch, B., Heuser, A., Eisenhauer, A., Spindler, M., Hemleben, C., 2009. A critical evaluation of calcium isotope ratios in tests of planktonic foraminifers. Geochim. Cosmochim. Acta 73, 7241-7255.

Gussone, N., Böhm, F., Eisenhauer, A., Dietzel, M., Heuser, A., Teichert, B.M.A., Reitner, J., Wörheide, G., Dullo, W.-C., 2005. Calcium isotope fractionation in calcite and aragonite. Geochim. Cosmochim. Acta 69, 4485-4494.

Gussone, N., Eisenhauer, A., Heuser, A., Dietzel,M., Bock, B., Böhm, F., Spero, H.J., Lea, D.W., Bijma, J., Nägler, T.F., 2003. Model for kinetic effects on calcium isotope fractionation

($\delta^{44}Ca$) in inorganic aragonite and cultured planktonic foraminifera. Geochim. Cosmochim. Acta 67, 1375-1382.

Hinrichs, K.-U., Summons, R.E., Orphan, V., Sylva, S.P., Hayes, J.M., 2000. Molecular and isotopic analysis of anaerobic methane-oxidizing communities in marine sediments. Org. Geochem. 31, 1685–1701.

Hippler, D., Schmitt, A.-D., Gussone, N., Heuser, A., Stille, P., Eisenhauer, A., Nägler, T. F., 2003. Ca isotopic composition of various standards and seawater. Geostandard Newslett. 27(1), 13-19.

Judd, A.G., Hovland, M., 2007. Seabed fluid flow. Cambridge University Press, New York, 360 pp.

Kastner, M., Claypool, G., Robertson, G., 2008. Geochemical constraints on the origin of the pore fluids and gas hydrate distribution at Atwater Valley and Keathley Canyon, northern Gulf of Mexico. Mar. Petr. Geol. 25, 860-872.

Kim, S.-T., O'Neil, J.R., 1997. Equilibrium and nonequilibrium oxygen isotope effects in synthetic carbonates. Geochim. Cosmochim. Acta 61(16), 3461-3475.

Koga, Y., Nishihara, M., Morii H., Akagawa-Matsushita, M., 1993. Ether polar lipids of methanogenic bacteria: structures, comparative aspects, and biosyntheses. Microbiol. Rev. 57, 164–182.

Lemarchand, D., Wasserburg, G.J., Papanastassiou, D.A., 2004. Rate-controlled calcium isotope fractionation in synthetic calcite. Geochim. Cosmochim. Acta 68, 4665-4678.

Lin, Z.Y., Sun, X.M., Lu, Y., Strauss, H., Xu, L., Gong, J.L., Teichert, B.M.A., Lu, R.F., Lu, H.F., Sun, W.D., Peckmann, J., 2017. The enrichment of heavy iron isotopes in authigenic pyrite as a possible indicator of sulfate-driven anaerobic oxidation of methane: Insights from the South China Sea. Chem. Geol. 449, 15-29.

Lin, Z.Y., Sun, X.M., Peckmann, J., Lu, Y., Xu, L., Strauss, H., Zhou, H.Y., Gong, J.L., Lu, H.F., Teichert, B.M.A., 2016. How sulfate-driven anaerobic oxidation of methane affects the sulfur isotopic composition of pyrite: A SIMS study from the South China Sea. Chem. Geol. 440, 26-41.

Ludwig, K.R., 2008. Using Isoplot/Ex, Version 3.70. A geochronological toolkit for Microsoft Excel: Berkeley Geochronology Ctr. Spec. Pub. 4.

Lumsden, D.S., 1979. Discrepancy between thin-section and x-ray estimates of dolomite in limestone. J. Sediment. Petrol. 49, 429-436.

Marriott, C.S., Henderson, G.M., Belshaw, N.S., Tudhope, A.W., 2004. Temperature dependence of δ^7Li, δ^{44}Ca and Li/Ca during growth of calcium carbonate. Earth Planet. Sci. Lett. 222, 615-624.

Meister, P., McKenzie, J.A., Vasconcelos, C., Bernasconi, S., Frank, M., Gutjahrs, M., Schrag, D.P., 2007. Dolomite formation in the dynamic deep biosphere: results from the Peru Margin. Sedimentology 54, 1007-1031.

Naehr, T.H., Eichhubl, P., Orphan, V.J., Hovland, M., Paull, C.K., Ussler III, W., Lorenson, T.D., Greene, G., 2007. Authigenic carbonate formation at hydrocarbon seeps in continental margin sediments: a comparative study. Deep-Sea Res. II 54, 1268-1291.

Nielsen, L.C., Depaolo, D.J., 2013. Ca isotope fractionation in a high-alkalinity lake system: Mono Lake, California. Geochim. Cosmochim. Acta 118, 276-294.

Nielsen, L.C., Depaolo, D.J., De Yoreo, J.J., 2012. Self-consistent ion-by-ion growth model for kinetic isotopic fractionation during calcite precipitation. Geochim. Cosmochim. Acta 86, 166-181.

Niemann, H., Elvert, M., 2008. Diagnostic lipid biomarker and stable carbon isotope signatures of microbial communities mediating the anaerobic oxidation of methane with sulphate. Org. Geochem. 39, 1668-1677.

Ockert, C., Gussone, N., Kaufhold, S., Teichert, B.M.A., 2013. Isotope fractionation during Ca exchange on clay minerals in a marine environment. Geochim. Cosmochim. Acta 112, 374-388.

Peckmann, J., Thiel, V., 2004. Carbon cycling at ancient methane-seeps. Chem. Geol. 205, 443-467.

Peketi, A., Mazumdar, A., Joshi, R., Patil, D., Srinivas, P., Dayal, A., 2012. Tracing the paleo sulfate-methane transition zones and H2S seepage events in marine sediments: an application of C-S-Mo systematics. Geochem. Geophys. Geosyst. 13, Q10007. http://dx.doi.org/10.1029/2012GC004288.

Ruffine, L., Donval, J.P., Croguennec, C., Burnard, P., Lu, H., Germain, Y., Legoix, L., Bignon, L., Cagatay, M.N., Marty, B., Madre, D., Pitel-Roudaut, M., Henry, P., Géli, L., This issue. Multiple gas reservoirs are responsible for the gas emissions along the Marmara fault network. Deep-Sea Res. Pt. II

Ruffine, L., Germain, Y., Polonia, A., de Prunele, A., Croguennec, C., Donval, J.-P., Pitel-Roudaut, M., Ponzevera, E., Caprais, J.-C., Brandily, C., Grall, C., Bollinger, C., Geli, L.,

Gasperini, L., 2015. Pore water geochemistry at two seismogenic areas in the Sea of Marmara. Geochem. Geophys. Geosyst. 16, 2038-2057.

Schmitt, A.D., Chabaux, F., Stille, P., 2003. The calcium riverine and hydrothermal isotopic fluxes and the oceanic calcium mass balance. Earth Planet. Sci. Lett. 213, 503-518.

Seeber, L., Cormier, M.-H., McHugh, C., Emre, O., Polonia, A., Sorlien, C., 2006. Rapid subsidence and sedimentation from oblique slip near a bend on the North Anatolian transform fault in the Marmara Sea, Turkey. Geology 34(11), 933-936.

Seeberg-Elverfeldt, J., Schlüter, M., Feseker, T., Kölling, M., 2005. Rhizon sampling of porewaters near the sediment-water interface of aquatic systems. Limnol. Oceanogr. Methods 3(8), 361-371.

Sim, M.S., Bosak, T., Ono, S., 2011. Large sulfur isotope fractionation does not require disproportionation. Science 333, 74.

Solomon, E.A., Kastner, M., MacDonald, I.R., Leifer, I., 2009. Considerable methane fluxes to the atmosphere from hydrocarbon seeps in the Gulf of Mexico. Nat. Geosci. 2, 561-565.

Strauss, H., Des Marais, D.J., Hayes, J.M., Summons, R.E., 1992. Abundances and isotopic compositions of carbon and sulphur species in whole rock and kerogen samples. In: Schopf, J.W., et al. (Ed.), In the Proterozoic Biosphere — a Multidisciplinary Study. Cambridge University Press, Cambridge, pp. 711-798.

Suess, E., Torres, M.E., Bohrmann, G., Collier, R.W., Greinert, J., Linke, P., Rehder, G., Tréhu, A., Wallmann, K., Winckler, G., Zuleger, E.,1999. Gas hydrate destabilization: Enhanced dewatering, benthic material turnover and large methane plumes at the Cascadia convergent margin. Earth Planet. Sci. Lett. 170, 1-15.

Tang, J., Dietzel, M., Böhm, F., Köhler, S.J., Eisenhauer, A., 2008. Sr^{2+}/Ca^{2+} and $^{44}Ca/^{40}Ca$ fractionation during inorganic calcite formation: II. Ca isotopes. Geochim. Cosmochim. Acta 72, 3733-3745.

Tarutani, T., Clayton, R.N., Mayeda, T.K., 1969. The effect of polymorphism and magnesium substitution on oxygen isotope fractionation between calcium carbonate and water. Geochim. Cosmochim. Acta 33(8), 987-996.

Teichert, B.M.A., Johnson, J.E., Solomon, E.A., Giosan, L., Rose, K., Kocherla, M., Connolly, E.C., Torres, M.E., 2014. Composition and origin of authigenic carbonates in the Krishna-Godavari and Mahanadi Basins, eastern continental margin of India. Mar. Petr. Geol. 58, 438-460.

Teichert, B.M.A., Bohrmann, G., Suess, E., 2005. Chemoherms on Hydrate Ridge - unique microbially-mediated carbonate build-ups growing into the water column. Palaeogeogr. Palaeocl. 227, 67-85.

Teichert, B.M.A., Gussone, N., Torres, M.E., 2009. Controls on calcium isotope fractionation in sedimentary porewaters. Earth Planet. Sci. Lett. 279, 373–382.

Tipper, E.T., Schmitt, A.-D., Gussone, N., 2016. Global Ca cycles: coupling of continental and oceanic processes. In: Gussone, N., et al. (Ed.), Calcium Stable Isotope Geochemistry. Springer, 173-222.

Tipper, E.T., Gaillardet, J., Galy, A., Louvat, P., Bickle, M.J., Capmas, F., 2010. Calcium isotope ratios in the world's largest rivers: A constraint on the maximum imbalance of oceanic calcium fluxes. Global Biogeochem. Cy. 24, GB3019, doi:10.1029/2009GB003574.

Wachter, E.A., Hayes, J.M., 1985. Exchange of oxygen isotopes in carbon dioxide-phosphoric acid systems. Chem. Geol. 52, 365-374.

Wallmann, K., Linke, P., Suess, E., Bohrmann, G., Sahling, H., Schlüter, M., Dählmann, A., Lammers, S., Greinert, J., Mirbach, N.v., 1997. Quantifying fluid flow, solute mixing, and biogeochemical turnover at cold vents of the eastern Aleutian subduction zone. Geochim. Cosmochim. Acta 61, 5209-5219.

Vidal, L., Menot, G., Joly, C., Bruneton, H., Rostek, F., Çağatay, M.N., Major, C., Bard, E., 2010. Hydrology in the Sea of Marmara during the last 23 ka: Implications for timing of Black Sea connections and sapropel deposition. Paleoceanography, 25. PA1205, doi:10.1029/2009PA001735

Whiticar, M.J., 1999. Carbon and hydrogen isotope systematics of bacterial formation and oxidation of methane. Chem. Geol. 161, 291-314.

Wortmann, U.G., Bernasconi, S.M., Böttcher, M.E., 2001. Hypersulfidic deep biosphere indicates extreme sulfur isotope fractionation during single-step microbial sulfate reduction. Geology 29, 647.

Yoshinaga, M.Y., Holler, T., Goldhammer, T., Wegener, G., Pohlman, J.W., Brunner, B., Kuypers, M.M.M., Hinrichs, K.-U., Elvert, M., 2014. Carbon isotope equilibration during sulphate-limited anaerobic oxidation of methane. Nat. Geosci. 7, http://dx.doi.org/10.1038/ngeo2069.

Figures

Figure 1. Bathymetric map of the Sea of Marmara showing the tectonic framework and the coring location. NAF: North Anatolian Fault.

Figure 2. Seafloor photograph from ROV VICTOR6000 of the sampling location of MRS-DV5-PC01 and 04. White spots on the seafloor are microbial filaments. Bubbles indicated by white arrows emanate from holes in the ground.

Figure 3. Photograph of push core MRS-DV5-PC01 showing black, sulfidic sediments on top and light gray at the bottom. Photographs on the right side show the depth distribution of authigenic carbonates found in the sediments of the push core and their mineralogy (HMC = high Mg-calcite).

Figure 4. Sulfate and sulfide concentrations and sulfur and oxygen isotopic compositions of pore water sulfate of MRS-DV5-PC01. Note that for sulfide sulfur isotopic composition samples were pooled (dotted line). Samples at 0 cm depth are bottom water samples.

Figure 5. Reconstructed gas chromatograms from core MRS-DV5-PC04 (Çinarcik basin in the Sea of Marmara) at 2-4 cm sediment depth. a) Hydrocarbon fraction showing the presence of crocetane and unsaturated pentamethylicosenes (PMIs). is: perdeuterated n-tetracosane. b) Alcohol fraction showing archaeol and sn-2 hydroxyarchaeol (sn-2-OHAr). is: heneicosanol. c) Fatty acid (methyl ester) fraction showing *i/ai*-$C_{15:0}$, $C_{16:1\omega5}$, Me-$C_{16:0}$ and cy$C_{17:0}$ FAs. is: nonadecanoic acid.

Figure 6. The $\delta^{18}O_{SO4}$ versus $\delta^{34}S_{SO4}$ pore water values of MRS-DV5-PC01 in comparison with data from Feng et al. (2016) derived from carbonate-associated sulfate from aragonites

of a seep location in the Gulf of Mexico. VCDT-Vienna Canyon Diablo Troilite; VSMOW-Vienna Standard Mean Ocean Water.

Figure 7. Stable carbon isotopic composition of dissolved inorganic carbon (DIC) and of authigenic carbonate carbon with depth from MRS-DV5-PC01. Age indicated is mean isochron U/Th age of four aragonite samples. HMC: high-Mg calcite; SMTZ: sulfate-methane transition zone.

Figure 8. Stable carbon and oxygen isotopic composition of different authigenic carbonate mineralogies of MRS-DV5-PC01 and MRS-DV5-PC04. Dotted, stippled and solid line indicate the equilibrium value for aragonite and calcite corrected for the amount of Mol% $MgCO_3$ (Tarutani et al., 1969). HMC: high-Mg calcite.

Figure 9. Strontium (A) and calcium (B) isotopic composition of pore water, bottom water and authigenic aragonite from MRS-DV5-PC01 with depth. Black dots and line show Sr^{2+} and Ca^{2+} pore water concentration. SMTZ: sulfate-methane transition zone.

Figure 10. Major earthquakes (black circles) in the Marmara region from Ambraseys and Jackson (2000). Red circles are earthquakes in Çinarcik Basin. Gray area indicates age of aragonites from U-Th ages and proposed start of methane seepage at the studied location. Ms-surface wave magnitude.

Table 1. Alkalinity, sulfide, sulfate, Ca^{2+} and Sr^{2+} concentrations and carbon isotopic composition of dissolved inorganic, Ca^{2+} and Sr^{2+} isotopic composition, sulfur and oxygen isotopic composition of sulfate and sulfur isotopic composition of sulfide of pore and bottom waters.

Depth	Alkalinity	HS^-	$\delta^{13}C_{DIC}$	Ca^{2+}	$\delta^{44/40}Ca$	Sr^{2+}	$^{87}Sr/^{86}Sr$	Depth	SO_4^{2-}	$\delta^{34}S_{SO4}$	$\delta^{18}O_{SO4}$	STD	Depth	$\delta^{34}S_{HS^-}$	STD

(cm)	(mol/l)	(mmol/l)	(‰ PDB)	(mmol/l)	(‰ SRM 915a)	(µmol/l)		(cm)	(mmol/l)	(‰ CDT)	(‰ PDB)		(cm)	(‰ CDT)	
bottom water	n.d.	n.d.	n.d.	n.d.	2.03	n.d.	0.709172	bottom water	9.64	20.8	8.71	0.08		n.d.	
1.5	16.39	0.87	-1.68	8.13	2.10	65.11	0.709173	1.5	4.67	32.1	13.31	0.460	1.5-4.5	-8.9	0.132
2.5	15.05	1.04	n.d.	9.09	2.12	74.00	n.d.	2.5	5.45	28.1	12.55	0.010			
3.5	13.81	1.03	-11.02	8.73	2.11	73.20	0.709175	3.5	4.78	27.7	11.86	0.350			
4.5	18.45	1.26	n.d.	8.73	2.10	73.21	n.d.	4.5	4.64	33.2	15.56	0.590			
5.5	18.08	1.79	-16.09	7.75	2.16	70.43	0.709176	5.5	3.96	35.9	17.50	0.340	5.5-9.5	-8.6	0.236
6.5	19.38	1.86	-20.63	8.16	2.08	74.73	n.d.	6.5 - 7.5	4.00	31.6	15.09	0.450			
7.5	21.41	2.03	-26.27	7.46	2.14	75.10	0.709184								
8.5	21.54	1.80	-13.58	7.50	2.16	76.89	n.d.	8.5 - 9.5	3.48	30.0	14.27	0.18			
9.5	21.62	1.79	-26.79	7.39	2.12	77.84	0.709187								
10.5	25.80	1.12	n.d.	5.86	2.24	73.75	n.d.	10.5 - 11.5	1.84	27.5	12.91	0.06	10.5 - 11.5	1.9	0.166
11.5	26.16	1.04	-31.67	5.25	2.26	70.87	0.709190								

n.d.: not determined

Table 2. Carbon and sulfur content and organic carbon isotopic composition of sediments and description, mineralogy, carbon, oxygen, calcium and strontium isotopic composition of authigenic carbonates.

Sediment						**Authigenic Carbonate**					
Depth (cm)	TC (wt %)	TOC (wt %)	TIC (wt %)	TS (wt %)	$\delta^{13}C_{org}$ (‰ PDB)	description	mineralogy	$\delta^{13}C$ (‰ PDB)	$\delta^{18}O$ (‰)	$\delta^{44/40}Ca$ (‰ SRM 915a)	$^{87}Sr/^{86}Sr$
1.1	9.2	3.5	5.7	0.3	-60.93	thin crust	aragonite	-31.47	2.52	0.67	0.709186
2.9	8.4	3.9	4.5	0.4	-58.70	thin crust	aragonite	-30.03	2.54	0.64	0.709184
4.4	7.0	3.6	3.5	0.6	-53.42	thin crust	aragonite	-27.69	2.62	0.90	0.709186
5.9	4.3	2.3	2.0	0.9	-40.15	thin crust	aragonite	-30.05	2.62	0.90	0.709192
7.4	3.7	1.9	1.8	1.0	-35.74	nodular plate	aragonite	-29.52	2.55	0.75	0.709192
8.8	3.3	1.6	1.7	0.9	-34.58	nodule	calcite, aragonite	-30.95	3.38	n.d.	n.d.
10.3	3.1	1.4	1.7	1.0	-29.07	nodule	calcite, aragonite	-30.51	3.34	n.d.	n.d.
11.8	2.7	1.3	1.4	1.0	-26.07	nodule	aragonite, calcite	-32.05	2.79	n.d.	n.d.
12.5						thin crust	aragonite	-33.40	1.40	0.93	0.709185
						nodule	aragonite, calcite	-33.16	2.80	n.d.	n.d.

n.d.: not determined

Table 3. Concentrations and carbon isotopic compositions of microbial lipids detected in sediment core MRS-DV5-PC04.

	0-2 cm	2-4 cm		4-6 cm		6-8 cm	
	µg/g	µg/g	$\delta^{13}C$, ‰	µg/g	$\delta^{13}C$, ‰	µg/g	$\delta^{13}C$, ‰
Archaeal lipids							
Archaeol	nd	13.4	−114	nd	nd	nd	nd
*Sn*2-hydroxyarchaeol	nd	26.1	−112	nd	nd	nd	nd
Crocetane	0.21	0.81	nd	0.82	−111	0.69	−96
PMI:1[a]	0.26	0.82	nd	0.58	nd	0.24	nd
PMI:2	1.30	1.68	nd	1.13	−114	3.27	−113
PMI:3	0.95	2.66	nd	3.12	−108	4.68	−109

PMI:4	0.27	0.48	nd	0.75	−91	1.58	−109
Bacterial lipids							
i-$C_{15:0}$ FA	7.24	8.87	−92[b]	5.26	nd	4.20	nd
ai-$C_{15:0}$ FA	11.5	14.1	−92[b]	6.68	nd	5.15	nd
$C_{16:1\omega5}$ FA	33.1	43.3	−86[c]	15.6	nd	10.3	nd
10Me-$C_{16:0}$ FA	4.84	6.91	−95	1.96	nd	2.08	nd
cy$C_{17:0\omega5,6}$ FA	6.11	8.08	−93	2.96	nd	2.18	nd

nd: not determined

[a] Unsaturated pentamethylicosenes and the numeral refers to the number of double bonds.

[b] coelution of i-$C_{15:0}$ FA and ai-$C_{15:0}$ FA

[c] coelution with $C_{16:1\omega7}$ FA

Table 4. Measured U-Th data (+ 2 s) for authigenic carbonates (only pure aragonite) and activity ratios used for isochron age calculation.

Sample	Weight (mg)	^{238}U (ppm)	^{232}Th (ppb)	(^{230}Th / ^{232}Th) (activity)	(^{238}U / ^{232}Th) (activity)	(^{234}U / ^{238}U) (activity)	(^{232}Th / ^{238}U) (activity)	(^{230}Th / ^{238}U) (activity)	**Mean isochron age (yr B.P.)**	$\delta^{234}U$ (initial)
MRS-05-01_0cm	75.8	3.574 ± 0.004	8.82 ± 0.09	0.170 ± 0.003	1.36 ± 0.02	1.134 ± 0.001	0.0809 ± 0.0020	0.0650 ± 0.0030		
MRS-05-01_2.5cm	62.8	3.379 ± 0.004	8.122 ± 0.083	0.170 ± 0.005	1.370 ± 0.034	1.134 ± 0.003	0.0787 ± 0.0020	0.0553 ± 0.0040	**235 ± 60**	145 ± 16
MRS-05-01_4.5cm	58.6	1.973 ± 0.003	2.768 ± 0.038	0.683 ± 0.003	4.072 ± 0.041	1.121 ± 0.001	0.2118 ± 0.0026	0.1444 ± 0.0007		

		2		0	9			0		0				1		0	0		0	0		0			
MRS	2	.		.	3			.		.		9		0	.		.	1		0	0		0		
-05-	4	9		0	7		2	7		0		.		.	1		0	0		0	7		0		
01_7	.	6		0	.		.	2		0		6		0	3		0	3		0	5		0		
.5cm	7	1	±	4	7	±	3	9	±	6	±	5	±	1	5	±	1	7	±	2	3	±	6		

All calculations have used the half-lives measured by Cheng et al. (2013).
A mean isochron age (N=4) was calculated using a sediment end-member at secular equilibrium (i.e. activity ratio = 1 ± 0.5), and given an arbitrary 25% error based on previous estimates (Bayon et al., 2013).
Initial $\delta^{234}U = ([^{234}U/^{238}U]activity - 1)x1000$, based on isochron ^{230}Th age and corrected from detrital contamination.
B.P. stands for “Before Present” where the “Present” is defined as the year 1950 A.D.

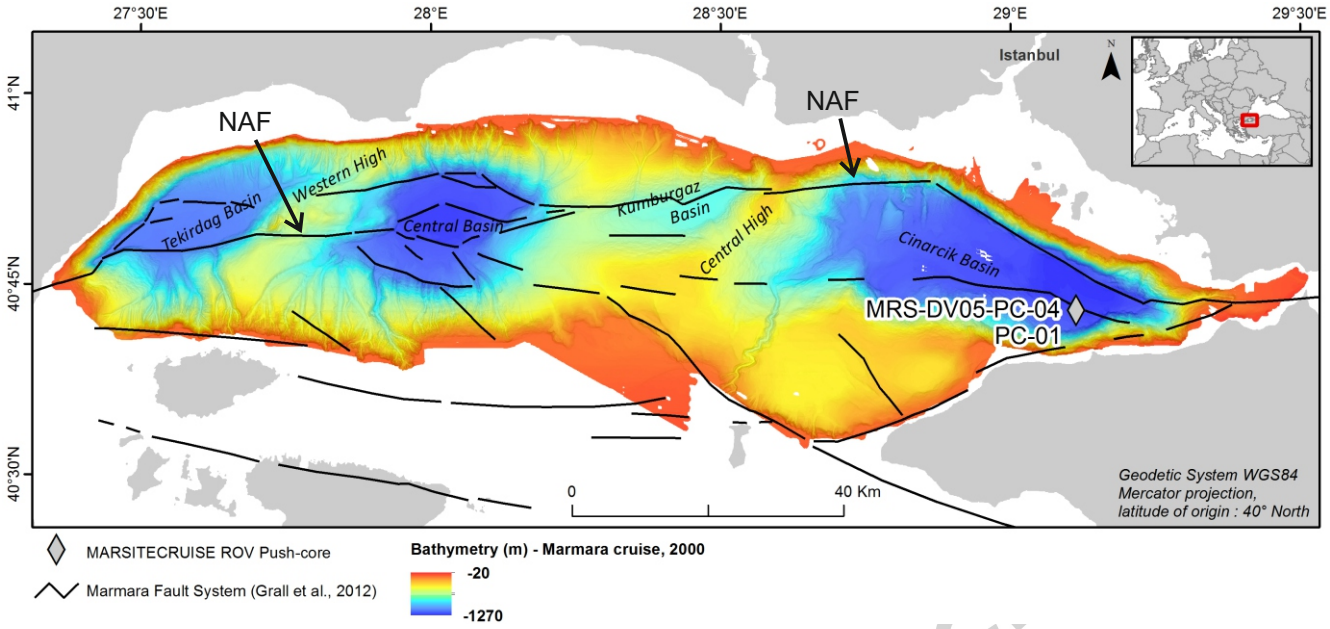

Figure 1

Teichert et al.

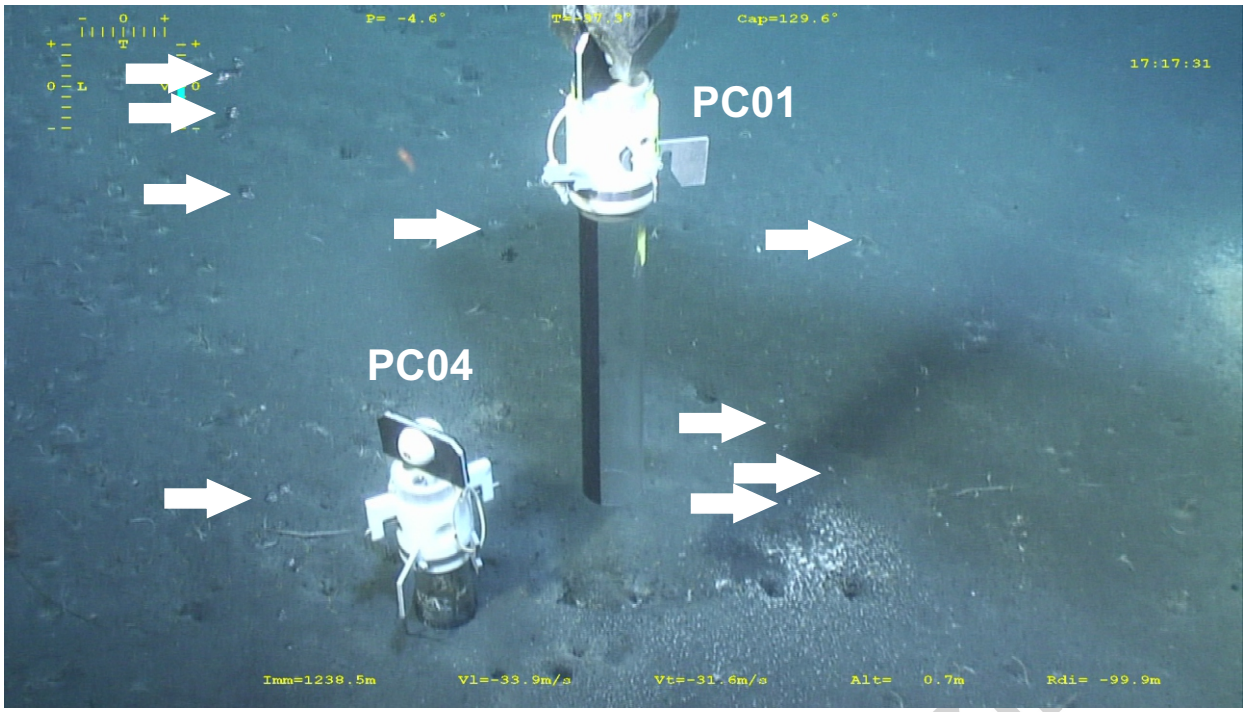

Figure 2

Teichert et al.

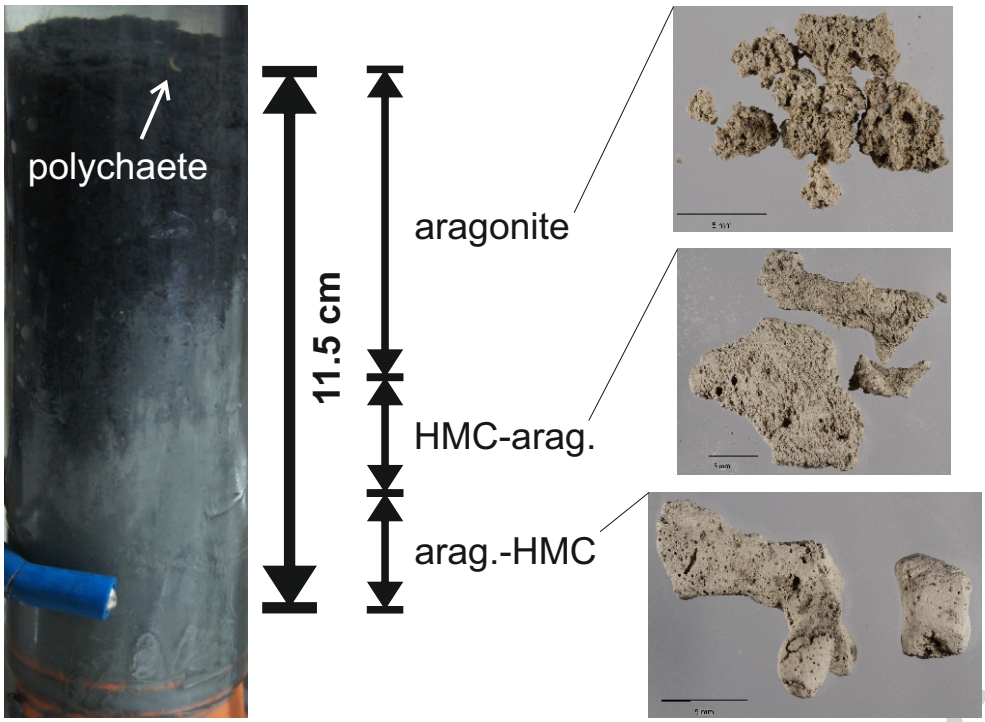

Figure 3

Teichert et al.

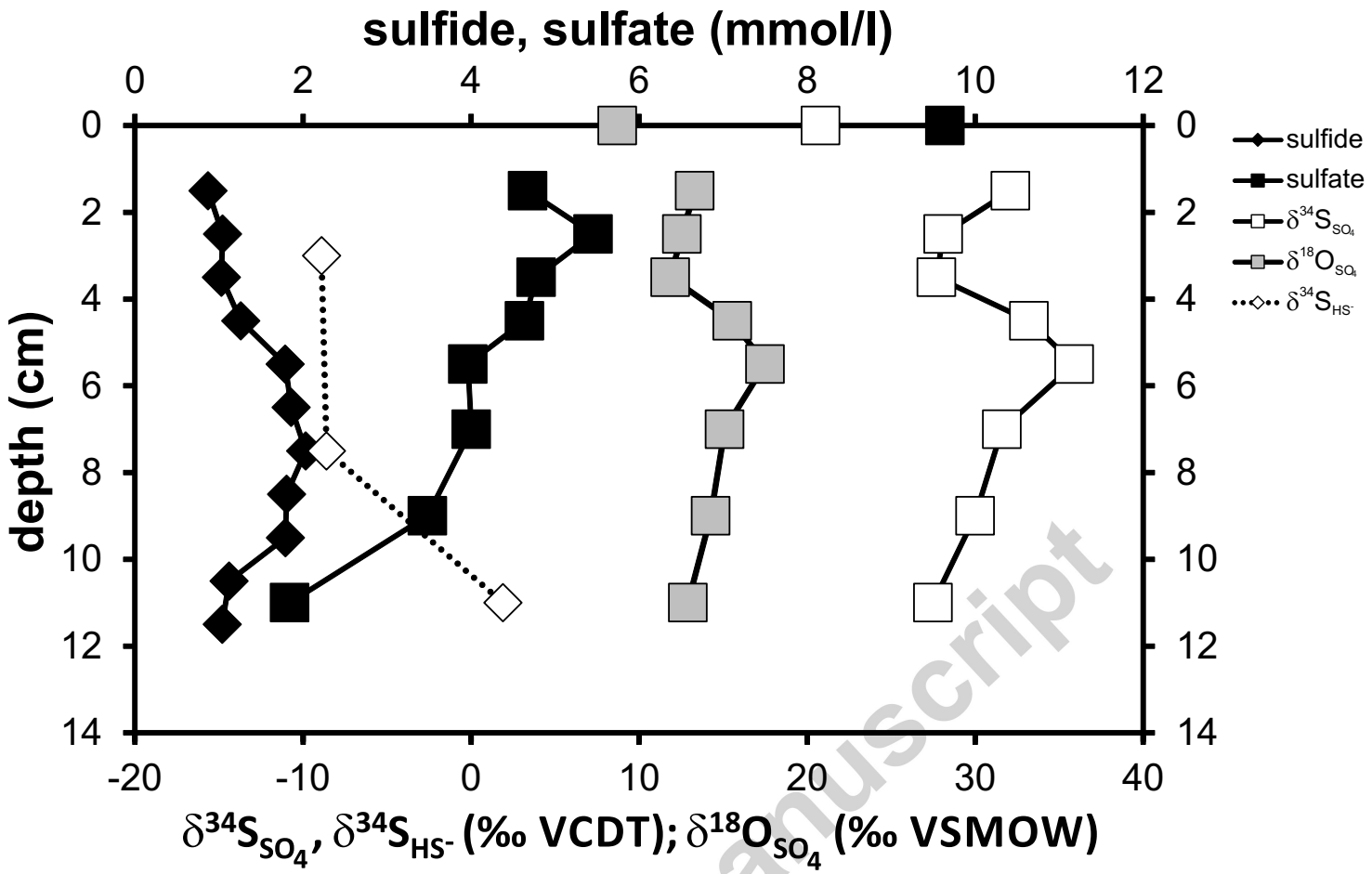

Figure 4

Teichert et al.

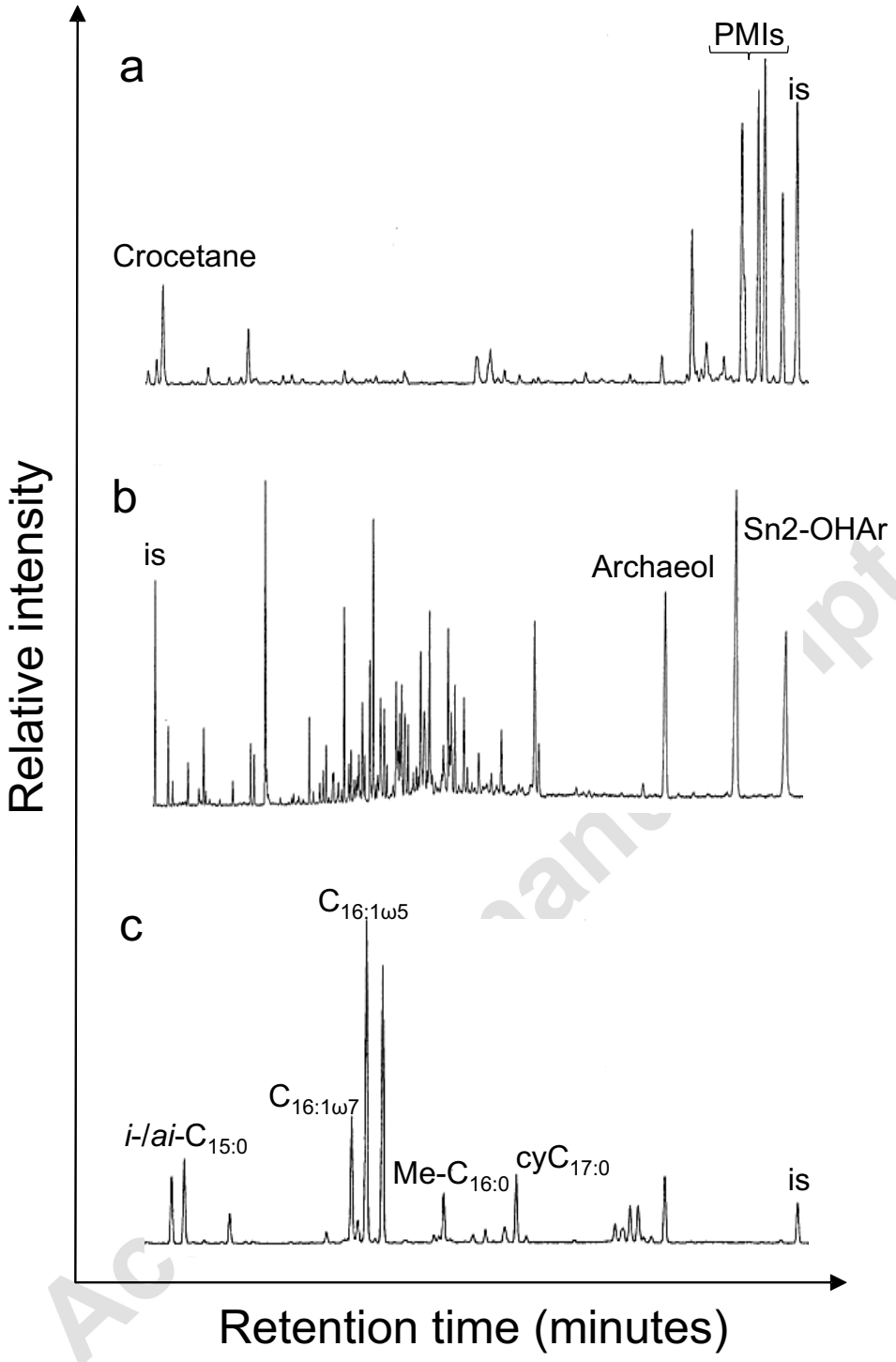

Figure 5

Teichert et al.

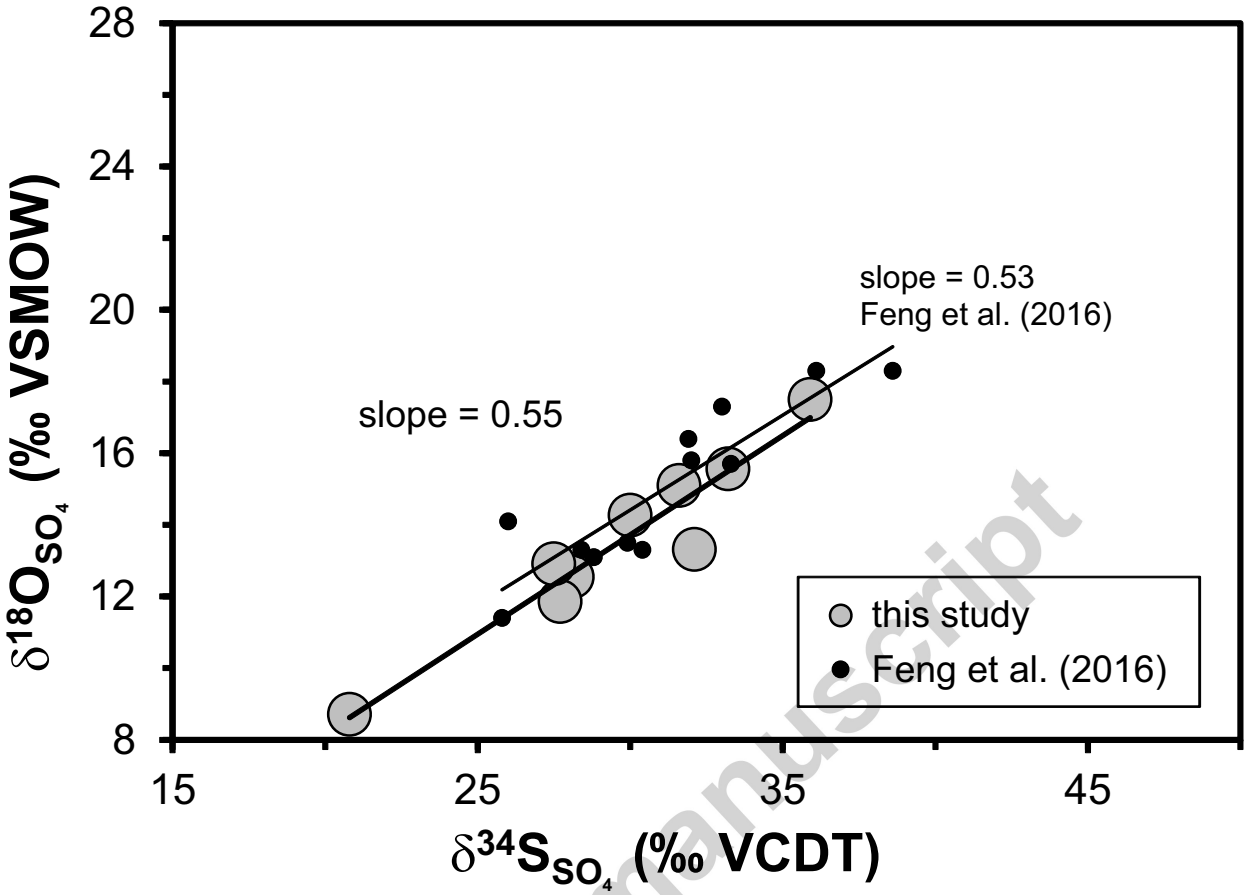

Figure 6

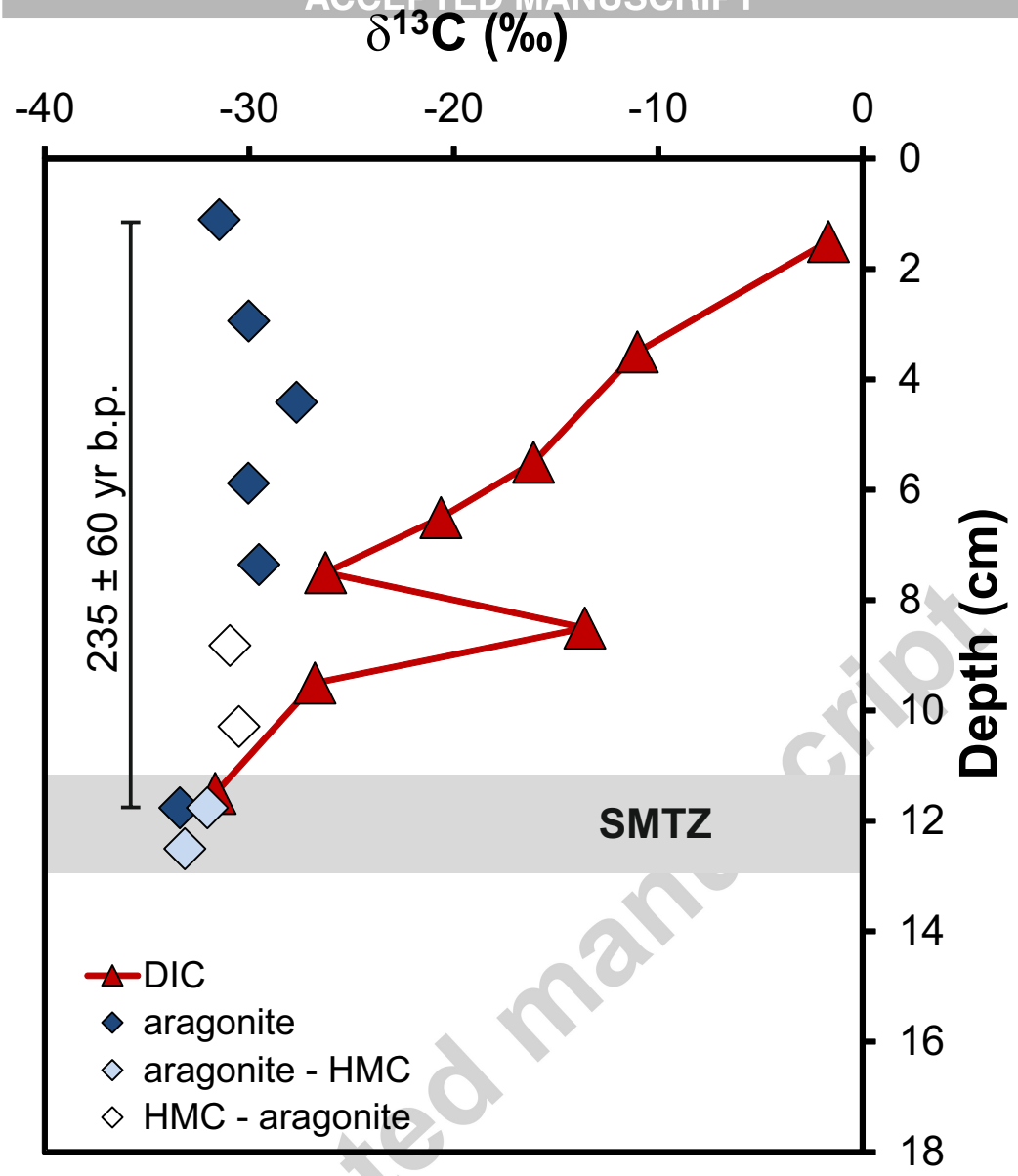

Figure 7

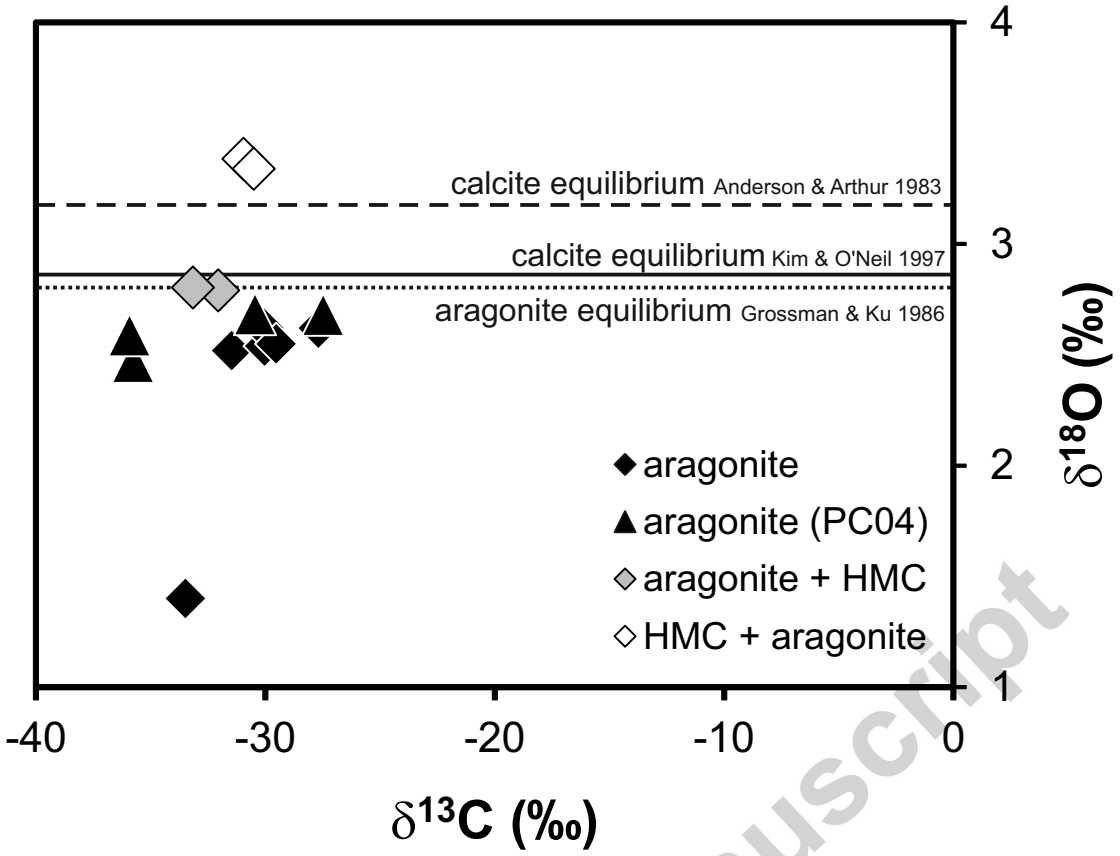

Figure 8

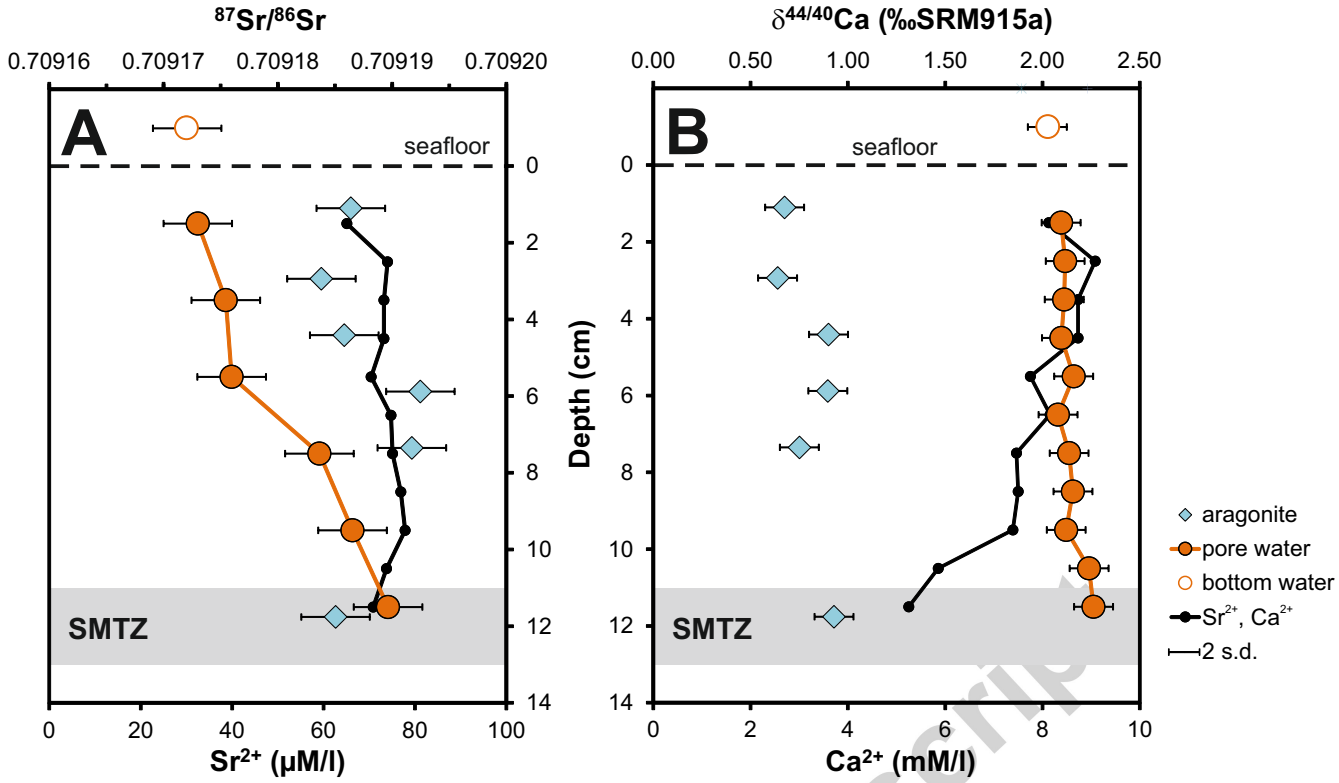

Figure 9

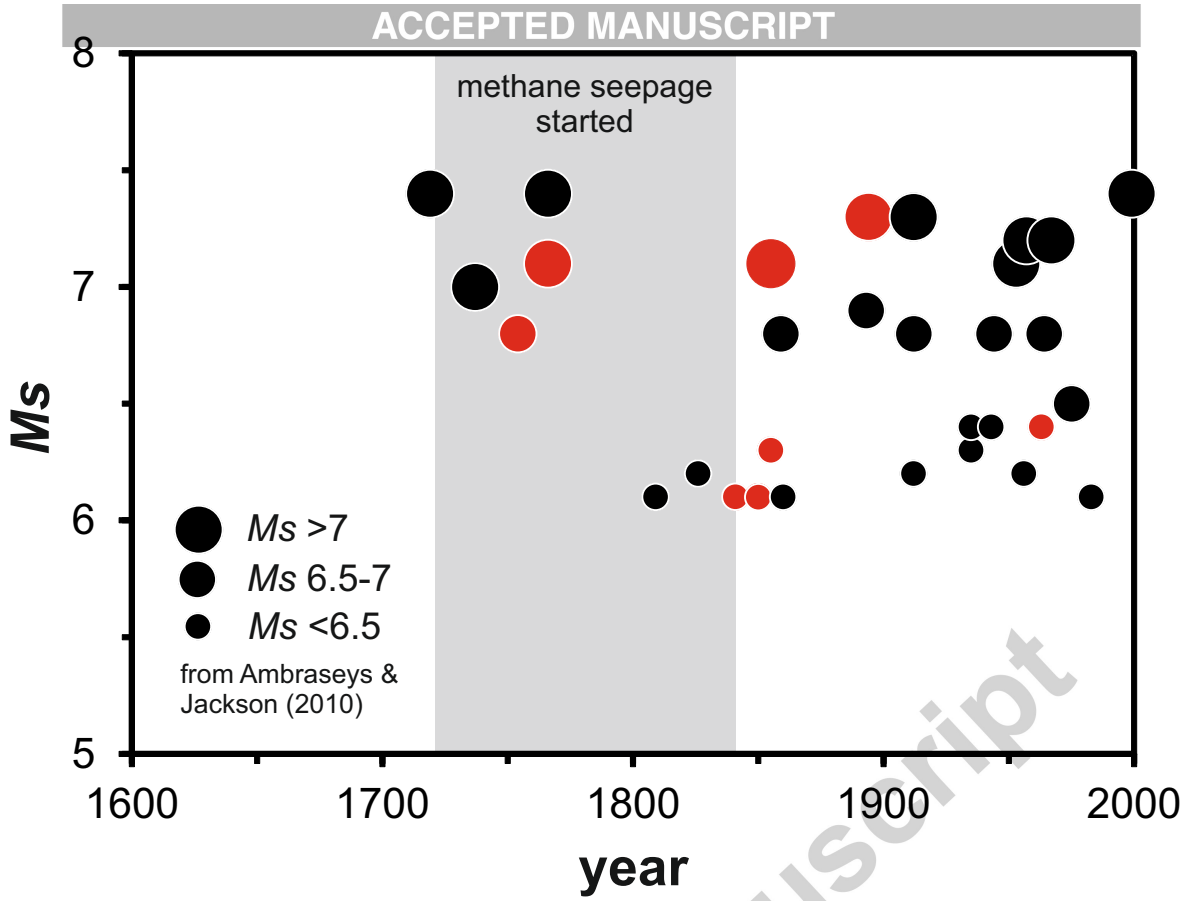

Figure 10

Teichert et al.